Published OnlineFirst June 29, 2015; DOI: 10.1158/0008-5472.CAN-15-0325

Integrated Systems and Technologies

Cancer Research

Endothelial Thermotolerance Impairs Nanoparticle Transport in Tumors

Alexander F. Bagley[1,2], Ruth Scherz-Shouval[3], Peter A. Galie[4], Angela Q. Zhang[1], Jeffrey Wyckoff[1], Luke Whitesell[3], Christopher S. Chen[4], Susan Lindquist[3,5,6], and Sangeeta N. Bhatia[1,6,7,8,9,10]

Abstract

The delivery of diagnostic and therapeutic agents to solid tumors is limited by physical transport barriers within tumors, and such restrictions directly contribute to decreased therapeutic efficacy and the emergence of drug resistance. Nanomaterials designed to perturb the local tumor environment with precise spatiotemporal control have demonstrated potential to enhance drug delivery in preclinical models. Here, we investigated the ability of one class of heat-generating nanomaterials called plasmonic nanoantennae to enhance tumor transport in a xenograft model of ovarian cancer. We observed a temperature-dependent increase in the transport of diagnostic nanoparticles into tumors. However, a transient, reversible reduction in this enhanced transport was seen upon reexposure to heating, consistent with the development of vascular thermotolerance. Harnessing these observations, we designed an improved treatment protocol combining plasmonic nanoantennae with diffusion-limited chemotherapies. Using a microfluidic endothelial model and genetic tools to inhibit the heat-shock response, we found that the ability of thermal preconditioning to limit heat-induced cytoskeletal disruption is an important component of vascular thermotolerance. This work, therefore, highlights the clinical relevance of cellular adaptations to nanomaterials and identifies molecular pathways whose modulation could improve the exposure of tumors to therapeutic agents.
Cancer Res; 75(16); 3255–67. ©2015 AACR.

Introduction

With the ongoing development of molecularly targeted therapies and nanoparticle carrier formulations, the delivery of such therapeutic cargos to solid tumors remains a central challenge in oncology. Locally enhancing the concentration of these agents within tumors will provide opportunities to achieve greater therapeutic efficacy, minimize off-target toxicities, and limit the development of drug resistance. Current chemotherapeutic regimens must carefully balance the conflicting goals of achieving cure and limiting systemic toxicity to normal organs. Many compounds, which are highly lethal to cancer cells *in vitro*, are rendered less effective in patients due to a narrow "therapeutic index," a constraint well appreciated in clinical oncology (1). To achieve the local concentrations required for optimal anticancer activity, the delivered cargo must overcome transport bottlenecks arising from physical features of tumors (e.g., high interstitial pressure and dense stroma; refs. 2, 3).

Perturbing the tumor vasculature represents an attractive approach for enhancing transport for at least two reasons. First, by regulating physical barriers, including blood flow and extravasation, the tumor vasculature limits the delivery of therapeutic agents spanning several orders of magnitude in size, including antibodies, nanoparticle carriers, and conventional chemotherapies (3–7). Second, many solid tumors are dependent on the host vasculature for supplying nutrients and oxygen during neoangiogenesis. These features make the vasculature a generalized and genetically stable target for solid tumors (8). Multifaceted efforts have been made to modify the tumor vasculature to enhance transport. The antiangiogenesis antibodies trastuzumab, bevacizumab, and cediranib normalize tumor vasculature, and thereby improve tumor blood flow (9–12). Transvascular transport is enhanced by VEGF, TNFα, IL1, histamine, and tumor-penetrating peptides (13–16). Physical approaches harnessing electromagnetic or acoustical energy (e.g., radiofrequency ablation or focused ultrasound) are also being actively explored (17–20). Nanomaterials (e.g., plasmonic nanoantennae) offer greater control of heating in tumor environments and have generated interest in nanomaterial-based methods for improving drug transport in tumors via localized heating (21–27). Plasmonic nanomaterials efficiently convert near-infrared light into localized heat due to rapid oscillations in the nanoparticle's electron cloud, an effect known as surface plasmon resonance (SPR; refs. 28, 29).

[1]Koch Institute for Integrative Cancer Research, Massachusetts Institute of Technology, Cambridge, Massachusetts. [2]MD-PhD Program, Harvard Medical School, Boston, Massachusetts. [3]Whitehead Institute for Biomedical Research, Cambridge, Massachusetts. [4]Departments of Bioengineering and Physiology, University of Pennsylvania, Philadelphia, Pennsylvania. [5]Department of Biology, Massachusetts Institute of Technology, Cambridge, Massachusetts. [6]Howard Hughes Medical Institute, Cambridge, Massachusetts. [7]Department of Electrical Engineering and Computer Science, Massachusetts Institute of Technology, Cambridge, Massachusetts. [8]Institute for Medical Engineering and Science, Massachusetts Institute of Technology, Cambridge, Massachusetts. [9]Broad Institute, Cambridge, Massachusetts. [10]Department of Medicine, Brigham and Women's Hospital, Boston, Massachusetts.

Note: Supplementary data for this article are available at Cancer Research Online (http://cancerres.aacrjournals.org/).

Corresponding Author: Sangeeta N. Bhatia, Massachusetts Institute of Technology, 77 Massachusetts Avenue, E19-502d, Cambridge, MA 02139. Phone: 617-253-0893; Fax: 617-324-0740; E-mail: sbhatia@mit.edu

doi: 10.1158/0008-5472.CAN-15-0325

Published OnlineFirst June 29, 2015; DOI: 10.1158/0008-5472.CAN-15-0325

Although many efforts have revealed how mass transport is altered in tumors as they develop, less is known about how the transport is altered in response to nanotherapeutic interventions, including hyperthermia (30, 31). Vascular thermotolerance represents a potentially important adaptation of tumors to heat and limits transport in tumors, yet the cellular and molecular components responsible for its effects are not well understood (5). Insight into how nanomaterial-mediated heating induces vascular thermotolerance and how vascular thermotolerance limits transport would deepen our understanding of tumor transport barriers and guide the development of oncologic approaches that use thermal energy.

The acquisition of thermotolerance has been primarily attributed to the heat-shock response (HSR), an evolutionarily conserved transcriptional program driven by heat-shock factor 1 (HSF1) to protect cells from damage to the proteome induced by high temperature (32). Upon heat shock, HSF1 binds to regulatory elements on the DNA and induces the transcription of HSPs, which act as molecular chaperones to restore protein homeostasis (33–35). Many aspects of this prosurvival response are conserved from yeast to human, in various stressful conditions. In cancer, HSF1 is activated in tumors to promote their survival. Recent studies have revealed two distinct transcriptional programs activated by HSF1 in cancer cells and in cancer-associated stromal cells. Not only are these transcriptional programs different from each other, they are also distinct from the classic transcriptional response induced by heat shock (35). Together, these two cancer-associated programs promote malignancy in ways that reach far beyond the activation of classical HSPs. In fact, when exposed to heat, cancer cells, and presumably other cell types in the tumor, are capable of mounting an additional HSR. However, it remains to be determined whether the HSR plays a role in mediating tumor transport through its effects on vascular thermotolerance.

Here, we explore the effects of local heating induced by plasmonic nanoantennae called gold nanorods (PEG-NRs) on tumor vasculature. PEG-NRs enhance the accumulation of therapeutic and diagnostic cargos in solid tumors, but at the same time they induce vascular thermotolerance. Therefore, although an initial heat exposure enhanced tumor transport, this effect was lost upon reexposure to PEG-NR–mediated heating (as would occur in clinical protocols requiring repeated administration of chemotherapeutics over periods of days to weeks). We demonstrate in ovarian tumor xenograft models that delivery of diffusion-limited therapeutic agents is impaired due to thermotolerance, contributing to diminished treatment responses. Using microfluidic endothelial permeability assays, *in vitro* analysis of the endothelial cytoskeleton, and intravital microscopy of the tumor vasculature, we identify the HSR as playing a primary role in limiting heat-induced disruption of the actin cytoskeleton, and thereby contributing to vascular thermotolerance. Finally, we preliminarily explore inhibition of the HSR as a remedy for thermotolerance using genetic approaches that diminish HSF1 activity. Collectively, we find rapid thermal adaptation of solid tumors to nanomaterial-generated heat stress, an effect with functional consequences for chemotherapeutic delivery and relevance to the design of more effective treatment schedules.

Materials and Methods

Animal models and cell lines

All studies involving mice were approved by the MIT Committee on Animal Care. Epithelial ovarian cancer models were established by unilateral or bilateral subcutaneous injection of approximately 1 to 2×10^6 CP70 human ovarian cancer cells into the rear flanks of 4- to 5-week-old athymic nude mice (Charles River Laboratories). The NOD-SCID *Hsf1*-null mouse model was generated in the Lindquist Laboratory, as follows: $Hsf1^{+/-}$ mice (BALB/c × 129SvEV), a gift from Ivor J. Benjamin (University of Utah, School of Medicine, Division of Cardiology, Salt Lake City, UT), were crossed with NOD-SCID mice, and intercrossed for four generations. Mice carrying a *SCID*/*SCID* genotype, in combination with either an $Hsf1^{+/+}$, $Hsf1^{+/-}$ or $Hsf1^{-/-}$ genotype were used for this study. The HGL heat-shock reporter mouse strain was generated in the Lindquist laboratory as follows: standard C57BL/6 ES cells were targeted with a plasmid encoding a GFP–Luciferase fusion protein, under regulation of the *HSPA6* promoter, and used to generate a mouse, which was then crossed into the albino variant and bred to homozygosity. $Rag1^{tm1Mom}$Tg(Tie2GFP)287Sato/J mice expressing GFP in endothelial cells were used for vessel permeability studies (The Jackson Laboratory). Tumor growth was monitored for approximately 10 to 20 days before injection of PEG-NRs. Human CP70 and OVCAR-8 cells were cultured in RPMI-1640 with L-glutamine (Invitrogen) supplemented with 10% FBS and penicillin/streptomycin. Mouse B16 melanoma cells were cultured in DMEM supplemented with 10% FBS and penicillin/streptomycin. Primary human umbilical vein endothelial cells (HUVEC) were cultured in media prepared from the EGM-2 BulletKit (Lonza).

PEG-NR synthesis

Concentrated cetyltrimethylammonium (CTAB)–coated gold nanorods (Nanopartz, Inc.) with dimensions of 41 × 10 nm were incubated with 5 kDa methyl-PEG-thiol (Laysan Bio, Inc.) to a final concentration of 100 μmol/L as described previously (36). After gentle mixing for 60 minutes, solutions were dialyzed for at least 24 hours in 3,500 MWCO Slide-A-Lyzer cassettes (Thermo Scientific) in deionized, distilled water. Solutions were transferred to 100 kDa filter tubes (Millipore) and washed with ultrapure water through five cycles of centrifugation (3,000 g, 10 minutes). PEG-NR solutions were resuspended in sterile PBS to an optical density of approximately 100 OD and stored at 4°C before use in animal models.

Tumor accumulation studies

Mice bearing bilateral CP70 ovarian tumors were administered i.v. injections of PEG-NRs (100 μL; 100–150 OD). After 48 to 72 hours to allow PEG-NR clearance from the systemic circulation, animals received an i.v. injection of AngioSpark750 (AS750; PerkinElmer; 50 μL in PBS; stock solution) and one flank tumor received 808 nm near-infrared irradiation for up to 30 minutes using a continuous 808 nm diode laser source (Visotek). Tumor temperature was monitored continuously with an infrared thermal camera (FLIR T650sc) and tumor temperature was maintained at 40°C to 43°C during the laser irradiation period. At multiple time points between 10 minutes and 48 hours after PEG-NR heating, tumor near-infrared fluorescence imaging was acquired using a whole-animal IVIS Spectrum-bioluminescent and fluorescent imaging system (Xenogen). Quantification of relative AS750 accumulation in PEG-NR–heated tumors compared with contralateral unheated tumors was performed using Living Image analysis software (v4.3.1). Tumors harvested from animals were rinsed in PBS and whole-tumor AS750 fluorescence was detected using a near-infrared imaging system (LICOR

Published OnlineFirst June 29, 2015; DOI: 10.1158/0008-5472.CAN-15-0325

Odyssey). Tumor homogenates were prepared by incubating tumor samples in tissue extraction buffer (70% EtOH, 0.3N HCl) and lysing samples on an automated homogenizer (gentleMACS Octo Dissociator, Miltenyi Biotec). Samples were centrifuged (1,000 rpm, 5 minutes), extracted overnight at 4°C, and supernatant fluorescence was measured in microplates on the LICOR imaging system.

For tumor accumulation studies in immunocompromised *Hsf1*-null, heterozygous, and wild-type animals, subcutaneous CP70 xenografts were established on the hind flank, PEG-NRs were administered i.v., and AS750 was administered immediately before heating. AS750 fluorescence was serially monitored by whole animal fluorescence imaging (IVIS) for up to 48 hours after injection. Area under the curve quantification was performed using GraphPad Prism software (v6.02).

Intravital imaging

Intravital tumor imaging was performed on an Olympus FV1000 multiphoton laser scanning confocal microscope with a ×25, N.A. 1.05 objective lens. For vessel permeability experiments, animals were anesthetized by isoflurane and administered an intravenous bolus of fluorescein dextran (70,000 MW; Invitrogen), tetramethylrhodamine dextran (2,000,000 MW; Invitrogen), or Texas Red dextran (70,000 MW; Invitrogen; 2–2.5 mg/mL). Immediately following injection of vascular dyes, tumors were positioned and immobilized on the stage for the duration of the experiment. For heat-shock induction experiments, dorsal window chambers were surgically implanted or skin-flap models were prepared in HGL reporter mice. Induction of the HSR as measured by GFP expression in vessels and surrounding tissue was monitored up to 24 hours after heating. For intratumoral cellular uptake studies, Rag1-Tie2GFP mice bearing unilateral subcutaneous CP70 xenograft tumors were i.v. administered TR-dextran to visualize the vessel lumen and interstitial cells and imaged with a ×25, N.A. 1.05 objective lens and ×4 digital zoom (×100 total magnification) within 1 to 2 hours following PEG-NR heating.

Microfluidic *in vitro* permeability studies

Microfluidic devices were fabricated as described previously (37, 38). Briefly, 400-μm stainless steel needles were withdrawn from collagen hydrogels polymerized within the device to create cylindrical voids that were then seeded with HUVECs. The endothelialized channels were exposed to continuously applied shear stress at magnitudes between 0.1 and 0.2 Pa for 12 to 18 hours to facilitate formation of tight junctions. Channels were placed in a temperature-controlled chamber (Air-Therm ATX, World Precision Instruments) on an epifluorescence microscope (Nikon Eclipse TI, Nikon Instruments). Saline solutions containing 70 kDa FITC-Dextran and Rhodamine-Dextran (Sigma) were continuously perfused through channels at flow rates of 5 μL/min. Temperature within the heated chamber was continuously monitored for the duration of each experiment. Fluorescence and brightfield images were acquired with a ×10 objective lens at the start and conclusion of each heating period. MetaMorph software (v7.7.3.0) was used for image acquisition. Channels receiving repeated heating cycles were returned to a 37°C incubator between the initial and subsequent imaging sessions, and again exposed to fluid shear stress. Dextran diffusion was quantified by tracking the movement of the dye front as a function of time. Image analysis, quantification of dye front displacement, and statistical analysis were performed with ImageJ software and GraphPad Prism software (v6.02).

Cytoskeletal stability studies

HUVECs were seeded into μ-Slide 8 Well standard bottom dishes (ibidi) at 4.5×10^3 cells per well and allowed to adhere for 24 hours. The culture medium was then exchanged for fresh medium containing rAVCMV-LifeAct-TagGFP2 adenovirus (multiplicity of infection: 100; ibidi). After overnight incubation at 37°C, HUVECs either received a heat pretreatment (45°C, 30 minutes) or were maintained at 37°C. Following a 24-hour recovery period at 37°C, all cells received a heat shock (45°C, 1 hour). Images were acquired using a ×20 objective lens on a fluorescence microscope (Nikon Eclipse Ti) before and 0, 1, 2, 4, and 6 hours after the final heat treatment. Images were obtained from 6 to 8 different wells per condition and time point. An investigator blinded to the experimental conditions scored cells contained visible actin filaments connecting nonadjacent points on the cell membrane, as well as the total number of cells per field. A total of 13,583 cells were scored (1,072–1,213 cells/condition) and statistical analysis was performed using GraphPad Prism software.

Cell viability studies

HUVECs were seeded at 5×10^3 cells per well in 96-well black glass-bottom plates (Grenier) and allowed to adhere for 24 hours. Cells were pretreated by incubation at 45°C for 30 minutes, allowed to recover for 24 hours at 37°C, then incubated at 45°C for an additional 1 hour. Cells were allowed to recover at 37°C for 30 hours. Relative viable cell number was assayed using Alamar Blue (Invitrogen) before and 0, 6, and 30 hours after the final heat treatment.

Tumor volume and survival studies

For tumor progression studies, nude mice were implanted with approximately 1×10^6 to 2×10^6 CP70 human ovarian cancer cells in the hind flanks. Tumor treatments consisted of administration of PEG-NRs, doxorubicin-loaded liposomes (5 mg/kg; Encapsula), and NIR irradiation with appropriate controls. Briefly, 48 to 72 hours after PEG-NR administration, tumors were exposed to NIR laser irradiation to achieve a temperature of approximately 41°C to 43°C for 30 minutes as monitored using an infrared camera (FLIR T650sc). Twenty-four hours later, animals underwent a second cycle of NIR laser irradiation in combination with intravenously administered doxorubicin-loaded liposomes. Longitudinal tumor progression studies lasted approximately 4 to 5 weeks from initial treatment with tumor volumes measured approximately every 3 to 4 days using digital calipers by investigators who were blinded to the experimental groups. Animals were euthanized when the tumor burden exceeded 500 mm^3. Plots and statistical analysis of tumor volume growth and Kaplan–Meier survival analysis were performed using GraphPad Prism.

Immunohistochemistry

Tumors were harvested and fixed in PBS containing 4% paraformaldehyde overnight at 4°C. Tissues were transferred to cassettes and placed in 70% ethanol solution at room temperature until paraffin embedding. Antibodies used included a rabbit polyclonal CD31 antibody (1:75, Abcam), rabbit monoclonal HSP70 (1:50, Cell Signaling Technology), and a cocktail of rat monoclonal antibodies to HSF1 (AB4; 1:500, Thermo Scientific). Slides were

Published OnlineFirst June 29, 2015; DOI: 10.1158/0008-5472.CAN-15-0325

counterstained with standard hematoxylin and eosin (H&E). LabVision Autostainer 360 Immunohistochemical Stainer (Thermo Scientific) was used to perform IHC with antigen retrieval.

Nanoparticle circulation time

AS750 and FITC-Dextran were i.v. administered to animals, and blood was collected by retro-orbital sampling at several times following injection using heparin-coated microcapillary tubes (VWR International). Samples were rapidly transferred to a 5 mmol/L EDTA solution to prevent coagulation. Blood samples were spun on a tabletop centrifuge for 30 to 60 seconds to separate plasma and erythrocyte fractions. Plasma fractions were transferred to 96-well plates and read on a fluorescence microplate reader (Molecular Devices) and near-infrared imaging system (LICOR).

Nanoparticle *in vitro* stability

AS750 nanoparticles were serially diluted in solutions of distilled water, PBS, 10% (v/v) FBS in PBS, and 50% (v/v) FBS in PBS to a lowest concentration of 1:100,000 of the stock concentration. Nanoparticle fluorescence was measured on an IVIS Spectrum-bioluminescent and fluorescent imaging system (Xenogen) and an Odyssey near-infrared scanner (LICOR). Image analysis and quantification was performed using ImageJ software.

Results

PEG-NR heating enhances tumor transport followed by development of thermotolerance

Mild heating of tumors with PEG-NRs or other methods has previously been shown to enhance the accumulation of diagnostic and therapeutic agents in tumors (5, 24, 39). To study the impact of nanomaterial-driven heating on tumor transport, mice with ovarian xenograft flank tumors were administered PEG-NRs several days before heating. At various times, tumor transport was assessed by quantifying delivery of pegylated fluorescent nanoparticles (AS750) as a model of diffusion-limited cargo. AS750 is composed of an iron oxide core coated with polyethylene glycol (PEG) and near-infrared fluorophores; its circulation time ($t_{1/2}$: 283 minutes), particle size (~35 nm), and spectral characteristics (Ex/Em: 750/775 nm) make it a good model for clinical nanoparticle formulations and for *in vivo* monitoring. Consistent with previous studies, tumors receiving a single exposure to PEG-NR heating accumulated AS750 in 2.1-fold excess compared with unheated tumors on the contralateral flanks (Fig. 1). Because most therapeutic agents are administered clinically in multiple cycles spanning periods of days to weeks, we explored the consequences of repeated PEG-NR heating on tumor transport. Ovarian tumor xenografts received repeated exposure to PEG-NR heating with intervals between heating episodes defined as Δt ranging from 8 hours to 1 week. Tumor transport was characterized at the time of the second heat exposure by administration of AS750. A Δt of 8 hours still resulted in a 1.4-fold increase in tumor transport relative to untreated tumors; however, the enhancement was reduced as compared with that seen after a single heat exposure. At longer Δt of 24 and 48 hours, tumor transport was no longer enhanced over untreated controls (0.9- and 1.0-fold, respectively), consistent with the development of vascular thermotolerance. At longer Δt, we noted a recovery of heat enhancement, beginning at 96 hours and increasing back to >2-fold by a Δt of 1 week. Fluorescence of explanted tumors displayed a similar trend, with shorter Δt between PEG-NR heat exposures correlating with reduced tumor transport (Supplementary Fig. S1). These data demonstrate that PEG-NR heating increases tumor transport but also induces a state of vascular thermotolerance that peaks at 24 to 48 hours and reverts after 1 week. In subsequent experiments, we used a Δt of 8 or 24 hours to further investigate the acquisition of thermotolerance within the tumor vasculature.

To explore the dynamics of heat-enhanced tumor transport, mice received either a single or double exposure to PEG-NR heating and tumor transport was assessed by offsetting the administration of AS750 by 0, 1, or 6 hours after heating (Supplementary Fig. S2A). Tumors receiving a single exposure of PEG-NR heating displayed a 2- to 2.7-fold increase in accumulation when AS750 was administered within 1 hour of PEG-NR heating and no relative enhancement in accumulation when AS750 was administered 6 hours after PEG-NR heating (Supplementary Fig. S2B and S2C). These data indicate that a

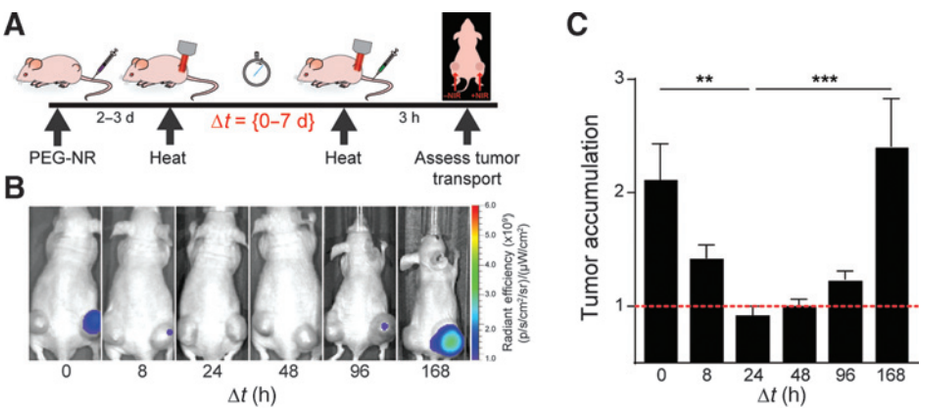

Figure 1.
Heat-induced transport enhancement is followed by a period of thermotolerance, wherein transport enhancement is resistant to subsequent heating. A, experimental time course included administration of gold nanorods (PEG-NR), an initial exposure of laser heating (heat), and an interval Δt varying from 0 to 7 days before reexposure (heat). Tumor transport was probed at the end of Δt via administration of AS750 imaging nanoparticles and tumor accumulation was quantified via *in vivo* fluorescence imaging. B, tumor transport as visualized by AS750 nanoparticle fluorescence in heated versus unheated tumors for increasing Δt. Note the increase in tumor transport after heat exposure was absent upon repeat exposure after 24 to 48 hours but began to recover at 96 hours. C, tumor transport (ratio of AS750 for heated vs. unheated tumors; $n = 8$–12/group from two independent experiments; **, $P < 0.01$; ***, $P < 0.001$, one-way ANOVA and Tukey post-tests); error bars, SE.

Published OnlineFirst June 29, 2015; DOI: 10.1158/0008-5472.CAN-15-0325

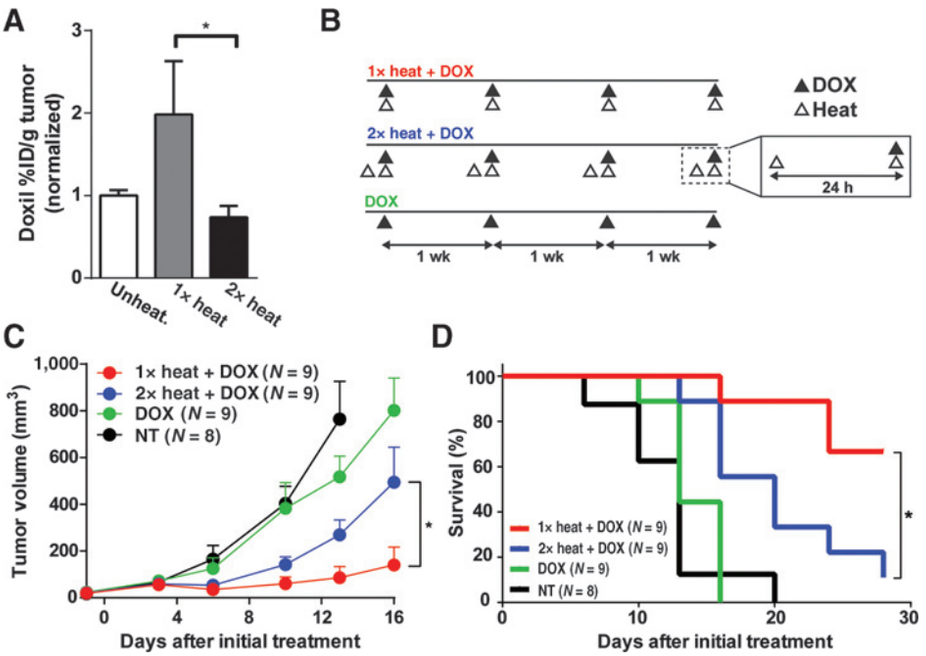

Figure 2.
Rational design of PEG-NR treatment regimens to enhance drug delivery and efficacy. A, accumulation of doxorubicin liposomes in unheated, single heat exposure (1× heat) and reexposure with Δt of 24 hours (2× heat) groups. Bars normalized to unheated controls. ($n = 5$ mice/group; *, $P < 0.05$, Mann–Whitney test); error bars, SE. B, time courses for each experimental group. Animals received 0, 1, or 2 exposures to PEG-NR heating with doxorubicin liposomes administered with the final heat exposure. Regimens were repeated weekly for the duration of the therapeutic trial period. C and D, tumor volume and Kaplan–Meier survival analysis [$n = 8$–9 mice/group; *, $P < 0.05$, unpaired t test, two-tailed, Holm-Sidak method for multiple comparisons (C) and log-rank Mantel–Cox test (D)]; error bars, SE.

single exposure of PEG-NR heating establishes a 6 hour "window" where nanoparticles can accumulate to a greater extent within heated tumors. Interestingly, in tumors receiving a repeated PEG-NR exposure after Δt of 8 hours, we no longer observed an enhancement in accumulation when AS750 was administered 1 hour following the second heat exposure (Supplementary Fig. S2B and S2C). These results suggest that both the magnitude of the thermal response and its dynamics may be altered after repeated exposure to heat. Taken together, these data demonstrate an initial increase in tumor transport in response to heat that is followed by a transient, reversible loss in heat enhancement.

Rational design of PEG-NR therapeutic regimens for enhanced tumor transport and efficacy

We next examined the relationship between PEG-NR–heating schedules, chemotherapeutic drug accumulation in tumors, and resulting anticancer activity. Our results in tumor models point to specific design criteria that could maximize the efficacy of combination approaches involving PEG-NR heating and chemotherapy. In particular, we reasoned that the temporal relationship between heating and administration of therapy may be important, as reexposure to PEG-NR heating with Δt of less than 96 hours dampened tumor accumulation. Doxorubicin-loaded liposomes are a clinically approved nanoparticle therapy for ovarian cancer, yet their relatively large particle diameter (~100 nm) limits their intratumoral accumulation. Consistently, a single exposure to PEG-NR heating led to a 2.7-fold higher concentration of doxorubicin liposomes in xenograft tumor homogenates relative to double heated tumors with Δt of 24 hours (Fig. 2A). Given the enhancement in intratumoral doxorubicin concentrations, we then investigated the degree to which improved delivery influenced antitumor efficacy, and animal survival. Cohorts of tumor-bearing mice were randomized to receive doxorubicin liposomes with either single or double exposures to PEG-NR heating (1× heat + Dox and 2× heat + Dox, respectively), doxorubicin liposomes alone (Dox), or no treatment (NT; Fig. 2B). We observed the greatest antitumor effect in the 1× heat + Dox cohorts. Although tumor growth was delayed in the 2× heat + Dox cohort relative to untreated controls, these tumors grew significantly faster than those in the 1× heat + Dox cohort (Fig. 2C). A similar trend was observed in a Kaplan–Meier survival analysis; untreated and Dox only cohorts survived between 16 and 20 days after initiation of treatment. Although 2× heat + Dox cohorts survived longer than either of these groups, the 1× heat + Dox cohorts survived for the longest duration overall and significantly longer than the 2× heat + Dox cohort with no evidence of systemic toxicity among any of the cohorts (Fig. 2D and Supplementary Fig. S3).

Endothelial response to PEG-NR heat exposure in the tumor environment

Because the endothelium is a dynamic, heat-responsive interface between the systemic circulation and the tumor interstitium, we next assessed the role of the endothelium in mediating vascular thermotolerance. Having observed the effect of thermotolerance on tumor transport and growth *in vivo*, we sought to visualize endothelial barrier function *in vivo*. In particular, we sought to understand the size dependence of the permeability effects on potential cargos, as well as observe endothelial responses to single and double PEG-NR heating in the tumor environment. Mouse xenograft models received either a single PEG-NR heat exposure or double PEG-NR heat exposure with a Δt of 24 hours. Transvascular transport in tumors was probed by an intravenous bolus of 70 kDa FITC-Dextran. Unheated tumors displayed minimal extravasation of 70 kDa FITC-Dextran tracer dye, whereas tumors receiving a single PEG-NR heat exposure exhibited vascular leakage into the interstitial space within an hour after heating (Supplementary Fig. S4). Consistent with bulk measurements in Fig. 1, tumors receiving a second exposure to PEG-NR heating displayed less extravasation of tracer dye into the interstitial space.

Published OnlineFirst June 29, 2015; DOI: 10.1158/0008-5472.CAN-15-0325

Increased vascular permeability via endothelial cell retraction would not necessarily lead to enhanced tumor accumulation of tracer due to bidirectional diffusive transport of cargo across the vessel wall (3). Therefore, we sought to understand what could be driving tracer accumulation and retention in our model using intravital microscopy. To visualize extravasation in proximity to tumor vessels at higher resolution, we established tumors in a transgenic mouse model using the Tie2 promoter to drive tissue-specific expression of GFP in endothelial cells. Intravenous 70 kDa Texas Red dextran (TR-Dex) was administered and the intra- and extravascular distribution of TR-Dex was examined in response to PEG-NR–heating regimens (Fig. 3). Most notably, we observed a significant number of perivascular TR-Dex–positive puncta, likely representing macrophage or dendritic cell populations, consistent with phagocytic uptake of TR-Dex (Fig. 3A and B). For each PEG-NR heating regimen, we quantified the frequency of TR-Dex–positive cells per volumetric image stack as a proxy for the degree of local extravasation (Fig. 3C). Unheated tumors displayed relatively few TR-Dex–positive cells, whereas tumors receiving a single exposure to PEG-NR heating displayed a significant 3.9-fold greater frequency of TR-Dex–positive cells. In contrast, tumors reexposed to PEG-NR heating with Δt of 24 hours displayed a reduced frequency of TR-Dex–positive cells, which was only 1.6-fold higher than the unheated state. For each condition, tumor blood flow was maintained during each imaging period, suggesting that vaso-occlusion or thrombosis was not a major contributor to the diminished extravasation observed with repeated PEG-NR heating (data not shown). Elevated levels of VEGF in the tumor microenvironment could also enhance vascular permeability, with both increased interendothelial gap formation and increased transcytosis. Nevertheless, we did not observe significant differences in VEGF expression following either heating regimen in this study (Supplementary Fig. S5).

To corroborate these observations with bulk tumor accumulation, tumor homogenates were prepared from mice injected i.v. with 70 kDa FITC-Dextran. Homogenates from tumors receiving a single exposure to PEG-NR heating accumulated 1.7-fold greater FITC-Dextran than unheated controls, whereas homogenates from tumors receiving a double heat exposure accumulated FITC-Dextran to a similar degree as unheated tumors (Fig. 3D).

Activation of endothelial HSR is sufficient to limit heat-enhanced transvascular transport

Having demonstrated a role for the endothelium in mediating vascular thermotolerance, we next focused on the relevant cellular and molecular pathways involved. To study the specific contribution of the endothelium to vascular thermotolerance, we used a microfluidic device consisting of a cylindrical channel lined by a

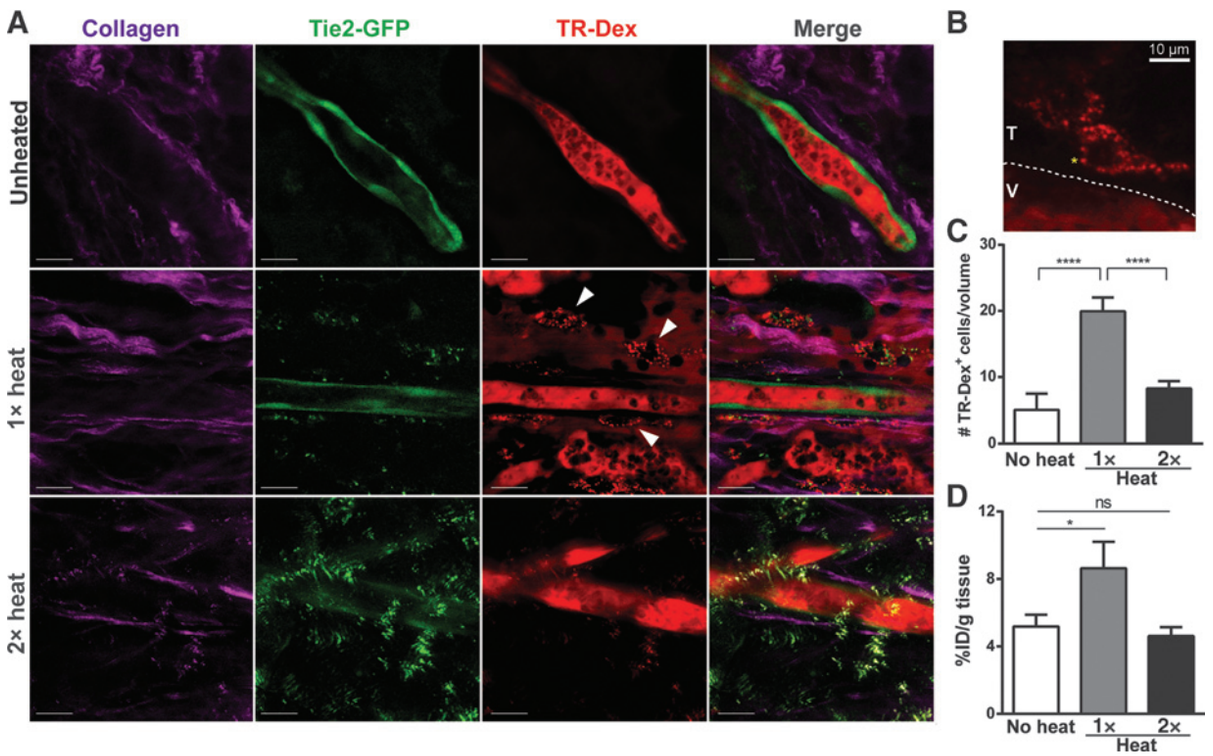

Figure 3.

Macromolecule accumulation *in vivo* after single or double PEG-NR–heating exposures. A, intravital imaging of intra- and extravascular distribution of 70 kDa Texas Red dextran (TR-Dex) in ovarian xenografts with Tie2-GFP^{+} endothelium. Collagen fibers (purple) highlight the tumor interstitial space, GFP (green) highlights tumor endothelium, and TR-Dex (red) is distributed between vessel lumen, interstitial space, and perivascular cells. PEG-NRs appear as punctate spots most strongly in GFP channel; scale bar, 20 μm. B, perivascular phagocytic cell residing in tumor interstitium (T) outside of tumor blood vessel (V). Yellow asterisk highlights uptake of TR-Dex cargo in putative endosome. C, quantification of TR-Dex–positive cells per tumor tissue volume measured by intravital imaging. (n = 15–23 fields of view from three mice per condition; ****, $P < 0.0001$, one-way ANOVA with Tukey post-tests); error bars, SE. D, accumulation of FITC-labeled 70 kDa Dextran in tumor homogenates from tumors receiving no heating, a single exposure, or double PEG-NR heat exposure. (n = 3–7 tumors/condition; *, $P < 0.05$, unpaired t test, two-tailed); error bars, SE.

Published OnlineFirst June 29, 2015; DOI: 10.1158/0008-5472.CAN-15-0325

monolayer of endothelial cells encapsulated in type I collagen (37). In Fig. 4A, the cylindrical monolayers represent a first approximation of the vasculature of solid tumors, which consist of an endothelial monolayer surrounded by a network of collagen fibers, proteoglycans, and cancer cells as well as reduced pericyte coverage (8). A saline solution containing 70 kDa FITC-Dextran was perfused through the endothelial channel and permeability associated with various temperatures and heating regimens was measured over time using the migration of the FITC-Dextran dye front (Fig. 4B). We applied a temperature ramp spanning physiologic body temperature of 37°C to 45°C to encompass the full range of temperatures achieved during *in vivo* PEG-NR–heating experiments. For vessels subjected to a single heat treatment, FITC-Dextran dye was retained within the vessel lumen between 38°C and 42°C (Fig. 4D and E). At 43°C, we observed significant migration of the dye front into the surrounding collagen matrix, indicating disruption of the endothelial monolayer and increased transvascular permeability (Fig. 4C). Structural changes to the endothelium were observed, as the cells transitioned from a confluent, flow-aligned "cobblestone" appearance before heating to a contracted state with increased frequency of interendothelial gaps (Fig. 4B).

Interestingly, when the same vessels were subjected to a second heat treatment with a Δt of 8 to 24 hours, the dye front displacement of FITC-Dextran was diminished. When heated channels were returned to physiologic body temperature after an initial heating, the endothelial cells resealed to form a functional barrier to FITC-Dextran diffusion (data not shown). Compared with their initial heating exposure, reheated vessels displayed 26.3- and 11.6-fold less dye front displacement at 42°C and 43°C, respectively (Fig. 4C and D). To integrate the effect across temperature, we calculated the cumulative dye front displacement during single heating and reheating regimens. The cumulative displacement of FITC-Dextran from the lumen into the surrounding collagen matrix between 40°C and 43°C was reduced by 2.6-fold in reheated channels relative to single heated channels (Fig. 4E). The ability to recapitulate vascular thermotolerance in a model containing minimal elements (i.e., endothelial cells and collagen) suggests that the endothelium is a key factor in adaptation to repeated thermal challenges.

Cytoskeletal recovery of endothelial cells is enhanced after repeated exposures to heat

The morphologic changes in endothelial cells suggested that cytoskeletal disruption can contribute to functional changes in permeability. To explore the response of the endothelial cytoskeleton to single versus double heat exposures, HUVECs were infected with adenovirus expressing an F-actin–binding GFP fusion protein, which enables dynamic monitoring of F-actin destabilization and structural recovery in living endothelial cells. HUVECs received either a single heat exposure ("1× heat") or second heat exposure with Δt of 24 hours ("2× heat"), and

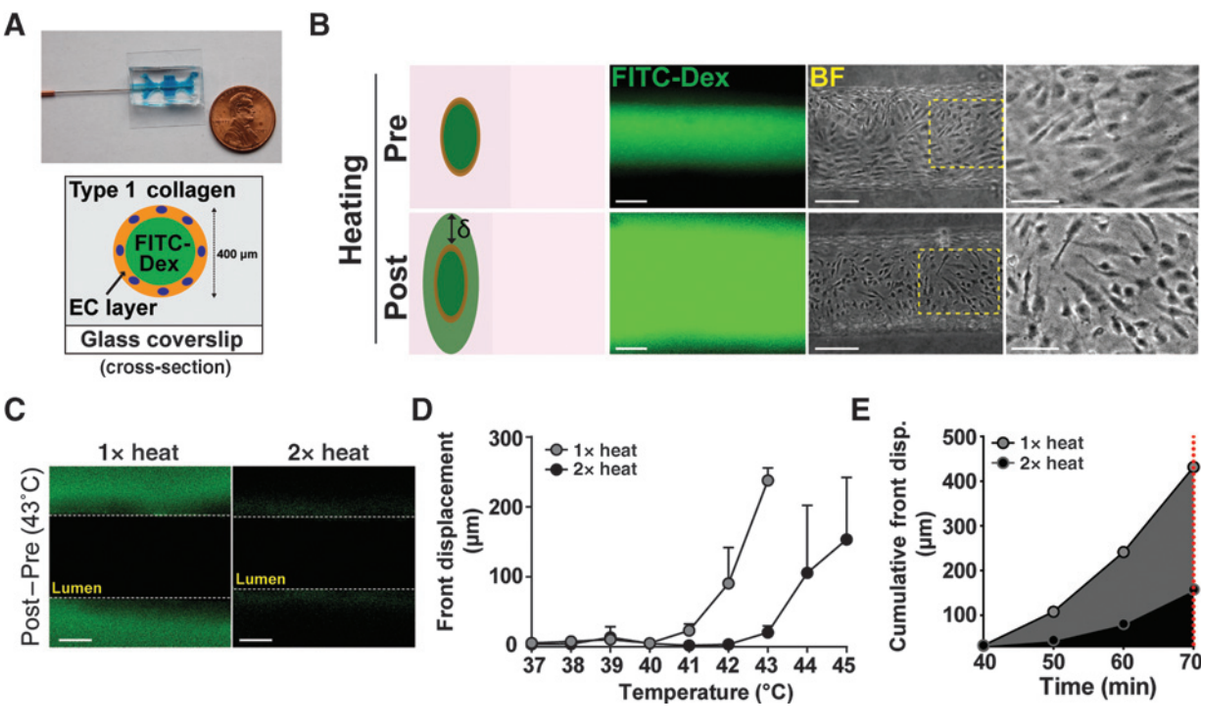

Figure 4.
Endothelial HSR is sufficient for transvascular transport and vascular thermotolerance. A, photograph and cross-section schematic of microfluidic endothelial channel. A cylindrical channel lined by an endothelial monolayer is established within a type 1 collagen gel. Saline solutions containing 70 kDa FITC-Dextran are flowed through the channel during controlled heating regimens to monitor temperature-dependent transport across endothelium. B, representative fluorescence and bright field images for pre- and post-heating. Dye front displacement (δ) measured for each temperature; scale bars, FITC-Dex, 200 μm; BF, 150 μm; BF zoomed, 75 μm. C, FITC-Dextran accumulation outside of lumen during 43°C heating period in microfluidic channels subjected to a single (1× heat) or repeated (2× heat) heat exposure; scale bar, 150 μm. D, dye front displacement versus temperature across physiologic temperature range ($n = 3$–6 channels/group). E, cumulative front displacement over time between 40°C and 43°C. Channels were exposed to each temperature level for 10 minutes, excluding ramping intervals.

Published OnlineFirst June 29, 2015; DOI: 10.1158/0008-5472.CAN-15-0325

cytoskeletal structure was serially monitored by time-lapse fluorescence microscopy (Fig. 5A). To quantify cytoskeletal structure, we scored cells with at least one visible F-actin filament connecting nonadjacent points along the cell membrane (F-Actin$^+$). Heating conditions were chosen to mimic the single and double PEG-NR–heating regimens explored *in vivo*, and the heat exposures in the minimal microfluidic vasculature *in vitro*. At physiologic temperatures, the majority of cells in the 1× and 2× heat groups displayed numerous membrane-spanning F-actin filament networks (Fig. 5B and D and Supplementary Fig. S6). Immediately following heating, both 1× and 2× heated cells displayed a collapsed F-actin appearance as observed in prior studies (40, 41). Time-lapse microscopy revealed the kinetics of cytoskeletal recovery of 1× and 2× heated cells following heat exposure. The 2×-heated endothelial cells exhibited efficient structural recovery 1 to 2 hours after heat exposure and remained stable at these levels for 4 to 6 hours after heat exposure. In contrast, 1× heated cells failed to exhibit recovery of the cytoskeleton 1 to 2 hours after heat exposure, and 6 hours later exhibited only partial recovery. Endothelial cell viability was not significantly different between 1× heated and 2× heated cells before heat exposure, immediately following heat exposure, or 30 hours following heat exposure. A small decrease in viability in 1× heated cells was observed 6 hours after heat exposure (Fig. 5C). Collectively, these data demonstrate that a preconditioning heat treatment of endothelial cells accelerates recovery upon subsequent heat exposure, which is manifested by more efficient F-actin cytoskeleton recovery. Importantly, the time scales for cytoskeletal recovery observed in 1× heated and 2× heated endothelial cell populations were similar to the windows of altered cargo accumulation observed in tumors exposed to single and double PEG-NR–heating regimens, respectively.

PEG-NR heat exposure induces a HSR

Because we found that vascular thermotolerance affects tumor transport, an understanding of the molecular pathways mediating this effect could suggest approaches to improve transport. The mammalian HSR is an ancient, evolutionarily conserved cellular signaling network that is activated in response to a variety of proteotoxic stresses, including heat, oxidative stress, low pH, and heavy metals (32). Previous studies have identified a role for the HSR in mediating thermotolerance in a variety of cells and organisms (42–44). Thermotolerance is classically defined as a cell-intrinsic adaptation to heat stress that promotes increased viability upon subsequent heat stress. Of interest to this study, thermotolerance has been shown to confer enhanced cytoskeletal stability to cells upon subsequent heat exposure (40, 41). To investigate whether nanomaterial-induced heat activates an HSF1-dependent HSR in our model, we performed intravital microscopy of tumor xenografts growing in transgenic mice expressing HSF1-dependent GFP fused to Luciferase (HGL model; Fig. 6A). HGL mice bearing B16 melanoma xenografts

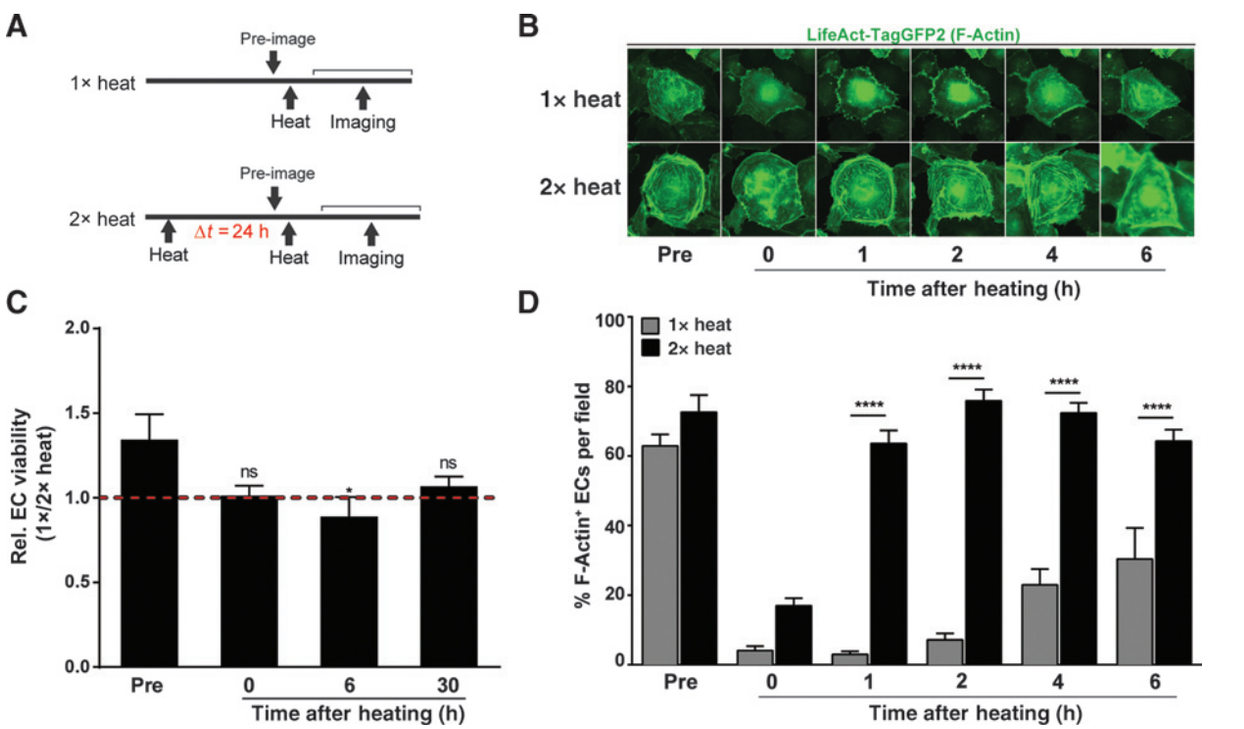

Figure 5.
Cytoskeletal recovery in endothelial cells is enhanced by preconditioning heat exposure. A, experimental time courses for single heat exposure (1× heat) and reexposure to heat (2× heat). B, representative fluorescence images of endothelial cell F-Actin filaments during recovery after final heating. Images depict cytoskeletal collapse and subsequent recovery. For each regimen, the same cell is shown across multiple time points to demonstrate the kinetics of endothelial cell recovery. C, relative endothelial cell (EC) viability for cells in 1× heat and 2× heat groups before and at different time points after heating. $n = 5$/group; *, $P < 0.05$, one-way ANOVA and Tukey post-tests. ns, nonsignificant. D, the percentage of cells with visible membrane-spanning F-Actin filaments per field during the post-heating recovery period. $n = 1{,}072$–$1{,}213$ cells from 6 to 8 fields of view per condition per time point; ****, $P < 0.0001$, two-way ANOVA and Bonferroni post-tests; error bars, SE.

Published OnlineFirst June 29, 2015; DOI: 10.1158/0008-5472.CAN-15-0325

received single PEG-NR heat treatments. Unheated tumors displayed minimal GFP expression in vascular territories (Fig. 6B). Because of their strong optical scattering properties, PEG-NRs were readily visualized in both heated and unheated tumors as punctate, perivascular signals in all emission channels (Fig. 6B and Supplementary Fig. S7). Tumors receiving a single PEG-NR heat exposure displayed a marked and diffuse increase in GFP expression in the host-derived tumor stroma, indicating robust induction of the HSR in response to PEG-NR heating. A cellular infiltrate appearing to concentrate the PEG-NRs in perivascular regions was also observed in PEG-NR–heated tumors (Fig. 6B). Using a dorsal skinfold model to investigate normal endothelium, several regions revealed strong vascular GFP expression, indicating that the normal vascular endothelium mounts a prominent HSR within hours following heating (Fig. 6C and D). Our results suggest that the thermotolerance we observed in tumors with Δt between 8 and 24 hours could be explained by induction of the HSR in the endothelium after an initial heat exposure. These experiments establish that tumor-localized heating by PEG-NRs and other means is sufficient to induce a robust HSR in both normal and tumor endothelium.

Inhibition of the HSR maintains heat-enhanced tumor transport upon repeated heating

We next investigated whether sustained inhibition of the HSR might restore transport in the setting of thermotolerance. To this end, we established tumor xenografts in immunocompromised mice harboring deletions in one or both alleles of *Hsf1*. Tumors received two PEG-NR heat exposures with a Δt of 24 hours. As in Fig. 1, AS750 tumor accumulation was serially measured by *in vivo* fluorescence imaging (Fig. 7A). Because we observed the greatest thermotolerance with Δt of 24 hours in earlier experiments, we selected this as the interval between PEG-NR heat exposures. Among the groups, animals with two functional alleles of *Hsf1* displayed the least enhancement in AS750 accumulation following 2× heating, consistent with the development of thermotolerance observed earlier (Fig. 7A and B). Interestingly, compared with $Hsf1^{+/+}$ mice, mice with one or two deleted *Hsf1* alleles accumulated 2.6- and 6.0-fold greater concentrations of AS750, respectively, during the 24 hours period following AS750 administration (Fig. 7C and D). To rule out the possibility that tumors growing in $Hsf1^{-/-}$ mice were more prone to accumulate AS750 than those growing in $Hsf1^{+/+}$ mice due to intrinsic, nonvascular structural differences, single exposures of PEG-NR heating were explored in $Hsf1^{+/+}$ and $Hsf1^{-/-}$ models. With single exposure to PEG-NR heating, we observed no significant difference in the net accumulation of AS750 in xenografts implanted in $Hsf1^{+/+}$ versus $Hsf1^{-/-}$ mice after 24 hours (Supplementary Fig. S8). Variations in accumulation based on genotype were observed at earlier time points (3–4 hours), but these differences were not statistically significant. Immunohistochemical staining of tumor sections revealed strong nuclear HSF1 expression in the tumor cells independent of the host's genetic background, but no expression in $CD31^{+}$ vascular cells in $Hsf1^{-/-}$ animals, even those that received PEG-NR heating (Supplementary Fig. S9). Collectively, these data suggest a model in which PEG-NR heating modulates the tumor endothelium in a transient, reversible manner, with consequences both for cargo delivery and overall therapeutic efficacy (Fig. 7E).

Discussion

This study deepens our understanding of vascular thermotolerance, both in terms of its functional effects on tumor growth and the underlying mechanisms involved. We find that nanomaterial-generated heat stress can induce vascular thermotolerance in tumors, contributing to reduced delivery of therapeutics and diminished treatment responses. In addition, we identify stabilization of the actin cytoskeleton associated with the endothelial HSR as a major feature of acquired vascular thermotolerance.

Because dosing regimens in the clinic require multiple cycles of administration, we explored the effect of reexposure to PEG-NR heating on tumor transport. Previous studies have elucidated a role for vascular thermotolerance in regulating tumor blood flow in a site- and tumor model–dependent manner (45). For instance, local vascular damage after heating in regions containing higher

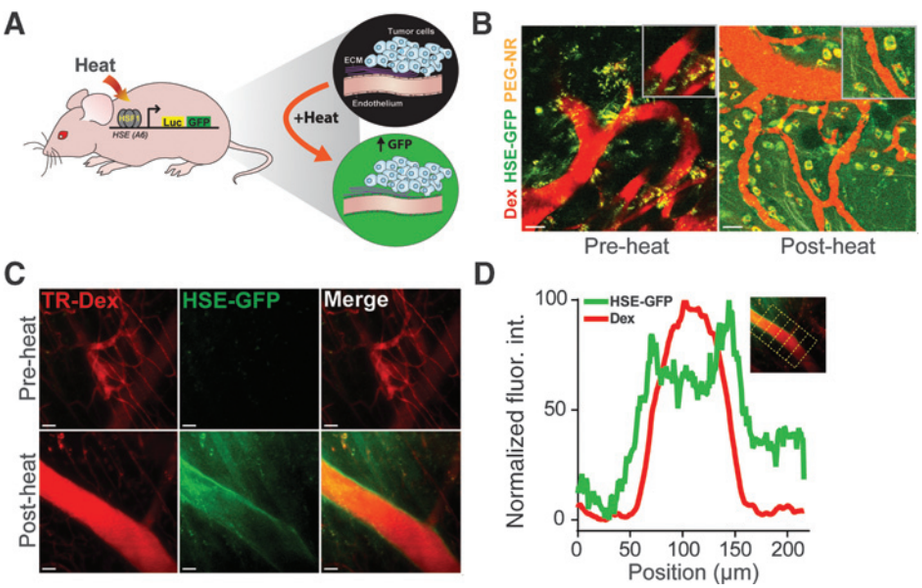

Figure 6.
Induction of HSR upon heating in tumor and normal vasculature. A, a schematic of HGL transgenic model. Heat-responsive promoter elements from the *HSPA6* gene regulate expression of GFP–firefly luciferase fusion protein, permitting visualization of the HSR in the host-derived tumor stroma, including the neovascular endothelium. B, elevated GFP expression following PEG-NR heating in tumors indicates robust induction of the HSR. Tumor vasculature highlighted by intravenous TR-Dextran (TR-Dex). Intrinsic luminescence of PEG-NRs allows for direct detection of nanoparticles by multiphoton microscopy. C and D, intravital imaging reveals induction of normal endothelial HSR. Line histogram profiles of normalized GFP and TR-Dex fluorescence intensities at regularly spaced intervals along vessel after heat exposure ($n = 6$ equidistant positions along vessel); scale bar, 50 μm

Published OnlineFirst June 29, 2015; DOI: 10.1158/0008-5472.CAN-15-0325

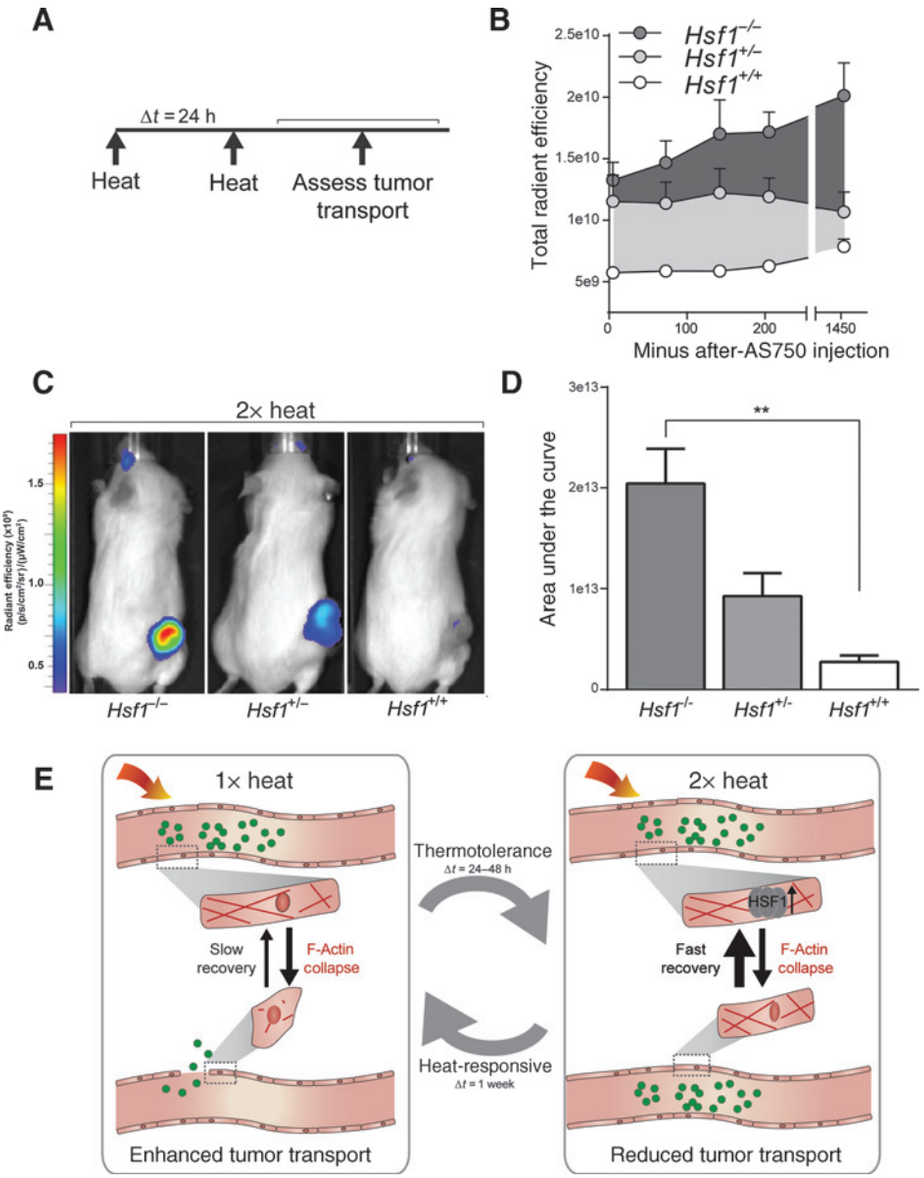

Figure 7.
Genetic ablation of HSR prevents vascular thermotolerance in response to repeated PEG-NR heating. A, ovarian tumor xenografts established in either homozygous-null (−/−), heterozygous (+/−), or wild type (+/+) *Hsf1* animals received an initial PEG-NR heat exposure (heat), an interval δt of 24 hours, and a reexposure to PEG-NR heating (heat). Tumor transport was assayed by i.v. injection of AS750 post-heating, followed by serial measurements of AS750 fluorescence for 24 hours by *in vivo* fluorescence imaging. B, tumor accumulation of transported AS750 for each genetic background up to 24 hour after treatment. $n = 3$–6/group; error bars, SE. C, representative *in vivo* fluorescence images in animals with $Hsf1^{-/-}$, $Hsf1^{+/-}$, and $Hsf1^{+/+}$ backgrounds receiving double PEG-NR heat exposures. D, area under the curve from panel B for each genetic background, demonstrating enhanced accumulation in $Hsf1^{-/-}$ animals. $n = 3$–6/group; **, $P < 0.01$, one-way ANOVA and Tukey post-tests; error bars, SE. E, the proposed model for the effects of PEG-NR heating on tumor transport and acquired thermotolerance. An initial exposure to PEG-NR heating alters the endothelial architecture via cytoskeletal collapse, leading to enhanced tumor transport of nanoparticle cargos. Over the next 24 to 48 hours, acquired thermotolerance, mediated by the HSR and *Hsf1*, upon reexposure to PEG-NR heating, results in enhanced cytoskeletal recovery and diminished tumor transport. Restoration of heat sensitivity occurs after approximately 1 week from the initial heat exposure.

concentrations of PEG-NRs may play a role in the initial development of vascular thermotolerance (30). In our model, however, the tumor vasculature remained functionally perfused with blood. Our studies extend the effects of vascular thermotolerance to transvascular transport, a major barrier to cargo delivery (46). Our data revealed a transient period of impaired transport in tumors reexposed to PEG-NR heating within 24 to 48 hours of an initial heat exposure. Heat responsiveness was restored approximately 1 week after the initial exposure. It is feasible that blood flow and transvascular transport in tumors are functionally coupled in the context of therapeutic delivery, and this hypothesis requires further study.

Our transport data enabled us to rationally design therapeutic dosing schedules involving PEG-NRs and chemotherapeutic agents. In particular, we observed that delivery of doxorubicin liposomes was impaired by vascular thermotolerance for a period of up to 48 hours. It is interesting that despite comparable therapeutic concentrations in the unheated and 2× PEG-NR–heating groups, animals receiving doxorubicin liposomes in combination with PEG-NR heating demonstrated slower tumor progression, which could reflect a synergistic interaction between heating and chemotherapy occurring in the tumor parenchyma. Nevertheless, the superior response to weekly doxorubicin liposomes and single PEG-NR heat exposure suggests that vascular thermotolerance has direct clinical consequences on tumor progression.

The well-defined role of the tumor endothelium in regulating cargo transport (3) led us to focus on its role in thermotolerance. Using a minimal microfluidic model of the endothelium, we recapitulated the transport behavior observed *in vivo*, providing evidence that the endothelium was sufficient for the development of thermotolerance. In addition, for both single and double heat

Published OnlineFirst June 29, 2015; DOI: 10.1158/0008-5472.CAN-15-0325

exposures, we linked the stability and recovery kinetics of the endothelium to F-actin cytoskeleton dynamics. Importantly, normal endothelial cells exhibited thermotolerance in our microfluidic and fluorescent actin studies, suggesting that this effect is not limited to tumor-associated endothelial cells. The *in vivo* selectivity for tumor vessels we observe is, therefore, likely a consequence of local PEG-NR accumulation and focused deposition of energy in the tumor environment, rather than intrinsic differences between normal and tumor endothelium; however, the similarity and differences in thermal responses of different endothelial subtypes remain an open area of inquiry. By observing similar heat-responsive kinetics at multiple biologic scales—from individual cells to three-dimensional endothelial models to the tumor environment—we suggest that subcellular processes in endothelial cells related to cytoskeletal stability contribute to the macroscopic effects on tumor transport.

Although the development of thermotolerance is associated with induction of the HSR, less is known about the role of the HSR in the context of therapeutic delivery. In this study, we demonstrate a role for the HSR in vascular transport by observing that induction of the HSR in the endothelium temporally correlates with the development of thermotolerance. Furthermore, genetic deletion of *Hsf1*, the master regulator of the mammalian HSR, in the vasculature was associated with enhanced accumulation following reexposure to PEG-NR heating. Loss of *Hsf1* in fibroblasts coinjected with breast cancer cells into mice has recently been shown to attenuate the growth of breast cancer tumor xenografts (47). CP70 cells used in this study, however, are a cisplatin-resistant, highly aggressive subclone of A2780 ovarian cancer cells. Xenografts formed by these cells are largely devoid of cancer-associated fibroblasts, and any other stroma, and still form in *Hsf1* null mice. A role for the HSR in endothelial stability has been suggested by previous reports identifying HSR proteins, including HSP27 as stabilizers of F-actin stress fibers during thermal stress (40, 41). Cell lines with elevated HSP27 expression had increased stability of stress fibers during multiple heat exposures. This behavior persisted for several days and contributed to maintenance of both normal morphology and viability. Future studies may illuminate roles of HSP27 and other HSR-regulated proteins in modulating transport across the vascular endothelium into the tumor.

Our focus in this study on the endothelial cell–intrinsic adaptations to heat exposure does not preclude other mechanisms of vascular permeability. In addition to thermally induced cytoskeleton collapse, endothelial contraction in venules is induced by vasoactive agents such as histamine and bradykinin, as well as cytokines, including TNF and IFNγ (48). Mast cell activation in tumors may induce local release of histamine, which in turn may contribute to the early phases (<1 hour) of enhanced nanoparticle delivery observed. In addition, direct endothelial injury in regions with high concentrations of PEG-NRs may induce an immediate sustained response lasting for several hours following PEG-NR heat exposure. VEGF influences vascular permeability in tumors (8), but we did not observe variations in VEGF between different heating regimens in this study. Finally, modifications to the extracellular matrix (ECM), particularly collagen, can independently modify drug transport (49–53). In our model, we observed retention of macromolecules in regions with higher collagen density (Supplementary Fig. S10), further supporting a role for the ECM in modulating drug transport. PEG-NR–mediated therapy alters collagen structure at ablative temperatures (54), but the effect at milder heating regimes remains an active area of investigation. The kinetics of nanoparticle accumulation suggest that vascular-modifying effects of PEG-NR heating are likely to be multifactorial, including both chemical mediators and the cell-intrinsic adaptations we describe.

Delivery of therapeutics to solid tumors in an efficient and specific manner remains a major challenge. In addition to molecular-targeting approaches with monoclonal antibodies or peptides, physical stimuli such as acoustic and electromagnetic energy have garnered interest because they target a genetically stable component of solid tumors. In addition, the technologies to generate intratumoral heating have significantly matured during the past decades, with nanomaterials such as gold nanorods offering the promise of more targeted, homogeneous, controlled, and efficient deposition of thermal energy within tumor tissue (55). Pharmacologic strategies to render endothelial cells more heat responsive or block the induction of thermotolerance would create new opportunities to enhance chemotherapy efficacy. As nanomaterial-inspired approaches are developed to improve tumor transport, this work anticipates a potential clinical challenge and suggests methods for achieving a maximal therapeutic response through rationally designed dosing schedules. Future studies investigating cellular adaptations to nanomaterial-mediated perturbations in solid tumors will provide additional avenues for incorporating nanomaterials into clinical practice.

Disclosure of Potential Conflicts of Interest

No potential conflicts of interest were disclosed.

Authors' Contributions

Conception and design: A.F. Bagley, A.Q. Zhang, C.S. Chen, S. Lindquist, S.N. Bhatia

Development of methodology: A.F. Bagley, R. Scherz-Shouval, A.Q. Zhang, J. Wyckoff

Acquisition of data (provided animals, acquired and managed patients, provided facilities, etc.): A.F. Bagley, R. Scherz-Shouval, P.A. Galie, A.Q. Zhang, J. Wyckoff

Analysis and interpretation of data (e.g., statistical analysis, biostatistics, computational analysis): A.F. Bagley, A.Q. Zhang, L. Whitesell, S. Lindquist

Writing, review, and/or revision of the manuscript: A.F. Bagley, R. Scherz-Shouval, P.A. Galie, A.Q. Zhang, L. Whitesell, C.S. Chen, S. Lindquist, S.N. Bhatia

Administrative, technical, or material support (i.e., reporting or organizing data, constructing databases): A.F. Bagley

Study supervision: C.S. Chen, S.N. Bhatia

Acknowledgments

The authors thank Dr. Heather Fleming for her helpful suggestions on this article; the Koch Institute Core Facilities, in particular Michael Brown, Denise Crowley, and Kathleen Cormier from the Koch Institute Histology Core.

Grant Support

This study was supported in part by a Koch Institute Support Grant P30-CA14051 from the National Cancer Institute (Swanson Biotechnology Center) and a Core Center Grant P30-ES002109 from the National Institute of Environmental Health Sciences. This study was additionally supported by the Marie-D. & Pierre Casimir-Lambert Fund, US National Institutes of Health (UH3 EB017103, R01 EB000262, and U54CA151884, and MIT-Harvard Center of Cancer Nanotechnology Excellence. A.F. Bagley acknowledges support from the Harvard-MIT MD-PhD Program at Harvard Medical School and MSTP grant T32GM007753 from the National Institute of General Medical Sciences. R. Scherz-Shouval was supported by the Human

Published OnlineFirst June 29, 2015; DOI: 10.1158/0008-5472.CAN-15-0325

Frontiers Science Program, the Fulbright Program, and the Israel National Postdoctoral Award Program for Women in Science. S.N. Bhatia and S. Lindquist are HHMI Investigators.

The costs of publication of this article were defrayed in part by the payment of page charges. This article must therefore be hereby marked *advertisement* in accordance with 18 U.S.C. Section 1734 solely to indicate this fact.

Received February 3, 2015; revised April 26, 2015; accepted May 15, 2015; published OnlineFirst June 29, 2015.

References

1. Minchinton AI, Tannock IF. Drug penetration in solid tumours. Nat Rev Cancer 2006;6:583–92.
2. Chauhan VP, Jain RK. Strategies for advancing cancer nanomedicine. Nat Mater 2013;12:958–62.
3. Jain RK, Stylianopoulos T. Delivering nanomedicine to solid tumors. Nat Rev Clin Oncol 2010;7:653–64.
4. Thurber GM, Weissleder R. A systems approach for tumor pharmacokinetics. PLoS ONE 2011;6:e24696.
5. Kong G, Braun RD, Dewhirst MW. Characterization of the effect of hyperthermia on nanoparticle extravasation from tumor vasculature. Cancer Res 2001;61:3027–32.
6. Alvarez Secord A, Jones EL, Hahn CA, Petros WP, Yu D, Havrilesky LJ, et al. Phase I/II trial of intravenous Doxil and whole abdomen hyperthermia in patients with refractory ovarian cancer. Int J Hyperthermia 2005;21:333–47.
7. Kong G, Dewhirst MW. Hyperthermia and liposomes. Int J Hyperthermia 1999;15:345–70.
8. Hanahan D, Weinberg RA. Hallmarks of cancer: the next generation. Cell 2011;144:646–74.
9. Goel S, Wong AH, Jain RK. Vascular normalization as a therapeutic strategy for malignant and nonmalignant disease. Cold Spring Harb Perspect Med 2012;2:a006486.
10. Jain RK. Normalization of tumor vasculature: an emerging concept in antiangiogenic therapy. Science 2005;307:58–62.
11. Kamoun WS, Ley CD, Farrar CT, Duyverman AM, Lahdenranta J, Lacorre DA, et al. Edema control by cediranib, a vascular endothelial growth factor receptor-targeted kinase inhibitor, prolongs survival despite persistent brain tumor growth in mice. J Clin Oncol 2009;27:2542–52.
12. Tong RT, Boucher Y, Kozin SV, Winkler F, Hicklin DJ, Jain RK. Vascular normalization by vascular endothelial growth factor receptor 2 blockade induces a pressure gradient across the vasculature and improves drug penetration in tumors. Cancer Res 2004;64:3731–6.
13. Sugahara KN, Teesalu T, Karmali PP, Kotamraju VR, Agemy L, Greenwald DR, et al. Coadministration of a tumor-penetrating peptide enhances the efficacy of cancer drugs. Science 2010;328:1031–5.
14. Brouckaert P, Takahashi N, van Tiel ST, Hostens J, Eggermont AM, Seynhaeve AL, et al. Tumor necrosis factor-alpha augmented tumor response in B16BL6 melanoma-bearing mice treated with stealth liposomal doxorubicin (DOXIL (R)) correlates with altered DOXIL (R) pharmacokinetics. Int J Cancer 2004;109:442–8.
15. Ten Hagen TLM, Van Der Veen AH, Nooijen PT, Van Tiel ST, Seynhaeve AL, Eggermont AM. Low-dose tumor necrosis factor-alpha augments antitumor activity of stealth liposomal doxorubicin (Doxil (R)) in soft tissue sarcoma-bearing rats. Int J Cancer 2000;87:829–37.
16. Ruegg C, Yilmaz A, Bieler G, Bamat J, Chaubert P, Lejeune FJ. Evidence for the involvement of endothelial cell integrin alpha V beta 3 in the disruption of the tumor vasculature induced by TNF and IFN-gamma. Nat Med 1998;4:408–14.
17. Liapi E, Geschwind JF. Transcatheter and ablative therapeutic approaches for solid malignancies. J Clin Oncol 2007;25:978–86.
18. Frenkel V. Ultrasound mediated delivery of drugs and genes to solid tumors. Adv Drug Deliv Rev 2008;60:1193–208.
19. O'Neill BE, Li KCP. Augmentation of targeted delivery with pulsed high intensity focused ultrasound. Int J Hyperthermia 2008;24:506–20.
20. ter Haar G. Therapeutic applications of ultrasound. Prog Biophys Mol Biol 2007;93:111–29.
21. Sershen SR, Westcott SL, Halas NJ, West JL. Temperature-sensitive polymer-nanoshell composites for photothermally modulated drug delivery. J Biomed Mater Res 2000;51:293–8.
22. Bartczak D, Muskens OL, Millar TM, Sanchez-Elsner T, Kanaras AG. Laser-induced damage and recovery of plasmonically targeted human endothelial cells. Nano Lett 2011;11:1358–63.
23. von Maltzahn G, Park JH, Agrawal A, Bandaru NK, Das SK, Sailor MJ, et al. Computationally guided photothermal tumor therapy using long-circulating gold nanorod antennas. Cancer Res 2009;69:3892–900.
24. Park J-H, von Maltzahn G, Xu MJ, Fogal V, Kotamraju VR, Ruoslahti E, et al. Cooperative nanomaterial system to sensitize, target, and treat tumors. Proc Natl Acad Sci U S A 2010;107:981–6.
25. Park JH, von Maltzahn G, Ong LL, Centrone A, Hatton TA, Ruoslahti E, et al. Cooperative nanoparticles for tumor detection and photothermally triggered drug delivery. Adv Mater 2010;22:880–5.
26. von Maltzahn G, Park JH, Lin KY, Singh N, Schwöppe C, Mesters R, et al. Nanoparticles that communicate *in vivo* to amplify tumour targeting. Nat Mater 2011;10:545–52.
27. Bagley AF, Hill S, Rogers GS, Bhatia SN. Plasmonic photothermal heating of intraperitoneal tumors through the use of an implanted near-infrared source. ACS Nano 2013;7:8089–97.
28. DasGupta D, von Maltzahn G, Ghosh S, Bhatia SN, Das SK, Chakraborty S. Probing nanoantenna-directed photothermal destruction of tumors using noninvasive laser irradiation. Appl Phys Lett 2009;95:233701.
29. Jain PK, Huang X, El-Sayed IH, El-Sayed MA. Noble metals on the nanoscale: optical and photothermal properties and some applications in imaging, sensing, biology, and medicine. Acc Chem Res 2008;41:1578–86.
30. Dewhirst MW, Vujaskovic Z, Jones E, Thrall D. Re-setting the biologic rationale for thermal therapy. Int J Hyperthermia 2005;21:779–90.
31. Thrall DE, Maccarini P, Stauffer P, Macfall J, Hauck M, Snyder S, et al. Thermal dose fractionation affects tumour physiological response. Int J Hyperthermia 2012;28:431–40.
32. Akerfelt M, Morimoto RI, Sistonen L. Heat shock factors: integrators of cell stress, development and lifespan. Nat Rev Mol Cell Biol 2010;11:545–55.
33. Sakurai H, Enoki Y. Novel aspects of heat shock factors: DNA recognition, chromatin modulation, and gene expression. FEBS J 2010;277:4140–9.
34. Pelham HR. A regulatory upstream promoter element in the Drosophila hsp 70 heat-shock gene. Cell 1982;30:517–28.
35. Mendillo ML, Santagata S, Koeva M, Bell GW, Hu R, Tamimi RM, et al. HSF1 drives a transcriptional program distinct from heat shock to support highly malignant human cancers. Cell 2012;150:549–62.
36. Lin KY, Bagley AF, Zhang AY, Karl DL, Yoon SS, Bhatia SN. Gold nanorod photothermal therapy in a genetically engineered mouse model of soft tissue sarcoma. Nano LIFE 2010;1:277–87.
37. Nguyen DH, Stapleton SC, Yang MT, Cha SS, Choi CK, Galie PA, et al. Biomimetic model to reconstitute angiogenic sprouting morphogenesis *in vitro*. Proc Natl Acad Sci U S A 2013;110:6712–7.
38. Galie PA, Nguyen DH, Choi CK, Cohen DM, Janmey PA, Chen CS. Fluid shear stress threshold regulates angiogenic sprouting. Proc Natl Acad Sci U S A 2014;111:7968–73.
39. Hauck ML, Dewhirst MW, Bigner DD, Zalutsky MR. Local hyperthermia improves uptake of a chimeric monoclonal antibody in a subcutaneous xenograft model. Clin Cancer Res 1997;3:63–70.
40. Lavoie JN, Gingras-Breton G, Tanguay RM, Landry J. Induction of Chinese hamster HSP27 gene expression in mouse cells confers resistance to heat shock. HSP27 stabilization of the microfilament organization. J Biol Chem 1993;268:3420–9.
41. Lavoie JN, Hickey E, Weber LA, Landry J. Modulation of actin microfilament dynamics and fluid phase pinocytosis by phosphorylation of heat shock protein 27. J Biol Chem 1993;268:24210–4.
42. Sanchez Y, Lindquist SL. Hsp104 required for induced thermotolerance. Science 1990;248:1112–5.
43. Lindquist S, Kim G. Heat-shock protein 104 expression is sufficient for thermotolerance in yeast. Proc Natl Acad Sci U S A 1996;93:5301–6.
44. Queitsch C, Hong SW, Vierling E, Lindquist S. Heat shock protein 101 plays a crucial role in thermotolerance in arabidopsis. Plant Cell 2000;12:479–92.

45. Gautherie M, et al. Biological basis of oncologic thermotherapy. Clinical thermology. Subseries thermotherapy. 1990, Berlin; New York: Springer-Verlag. p. 169.
46. Lin JC, Song CW. Influence of vascular thermotolerance on the heat-induced changes in blood-flow, Po2, and cell-survival in tumors. Cancer Res 1993;53:2076–80.
47. Scherz-Shouval R, Santagata S, Mendillo ML, Sholl LM, Ben-Aharon I, Beck AH, et al. The reprogramming of tumor stroma by HSF1 is a potent enabler of malignancy. Cell 2014;158:564–78.
48. Robbins SL, Kumar V, Cotran RS. Robbins and Cotran pathologic basis of disease. 8th ed. 2010, Philadelphia, PA: Saunders/Elsevier. p. 1450.
49. Chauhan VP, Martin JD, Liu H, Lacorre DA, Jain SR, Kozin SV, et al. Angiotensin inhibition enhances drug delivery and potentiates chemotherapy by decompressing tumour blood vessels. Nat Commun 2013;4:2516.
50. Diop-Frimpong B, Chauhan VP, Krane S, Boucher Y, Jain RK. Losartan inhibits collagen I synthesis and improves the distribution and efficacy of nanotherapeutics in tumors. Proc Natl Acad Sci U S A 2011;108:2909–14.
51. Mok W, Boucher Y, Jain RK. Matrix metalloproteinases-1 and -8 improve the distribution and efficacy of an oncolytic virus. Cancer Res 2007;67:10664–8.
52. Alexandrakis G, Brown EB, Tong RT, McKee TD, Campbell RB, Boucher Y, et al. Two-photon fluorescence correlation microscopy reveals the two-phase nature of transport in tumors. Nat Med 2004;10:203–7.
53. Brown E, McKee T, diTomaso E, Pluen A, Seed B, Boucher Y, et al. Dynamic imaging of collagen and its modulation in tumors *in vivo* using second-harmonic generation. Nat Med 2003;9:796–800.
54. Lo JH, von Maltzahn G, Douglass J, Park JH, Sailor MJ, Ruoslahti E, et al. Nanoparticle amplification photothermal unveiling of cryptic collagen binding sites. J Mater Chem B Mater Biol Med 2013;1:5235–40.
55. Wust P, Hildebrandt B, Sreenivasa G, Rau B, Gellermann J, Riess H, et al. Hyperthermia in combined treatment of cancer. Lancet Oncol 2002;3:487–97.

Cancer Research
The Journal of Cancer Research (1916–1930) | The American Journal of Cancer (1931–1940)

AACR American Association for Cancer Research

Endothelial Thermotolerance Impairs Nanoparticle Transport in Tumors

Alexander F. Bagley, Ruth Scherz-Shouval, Peter A. Galie, et al.

Cancer Res 2015;75:3255-3267. Published OnlineFirst June 29, 2015.

Supplementary Information for

Title: Endothelial thermotolerance impairs nanoparticle transport in tumors

Authors: Bagley AF, Scherz-Shouval R, Galie PA, Zhang AQ, Wyckoff J, Whitesell L, Chen CS, Lindquist S, Bhatia SN.

Figures:

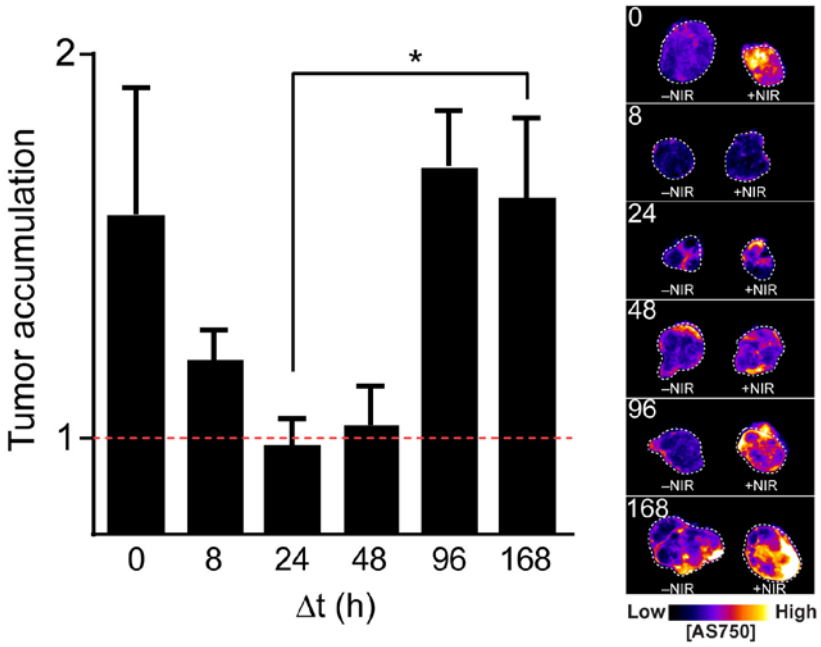

Supplementary Figure 1. Tumor accumulation of AS750 after PEG-NR heat exposure with varying delta T. Tumor transport (ratio of AS750 for cohorts of heated versus unheated tumors) and two representative images of tumors that were explanted after PEG-NR heating with delta T values ranging between 0 h to 1 week, and assayed by IVIS for AS750 transport. (n = 4-9 per group from two independent experiments, *P<0.05, one-way ANOVA and Tukey's post-tests.) Error bars, SE.

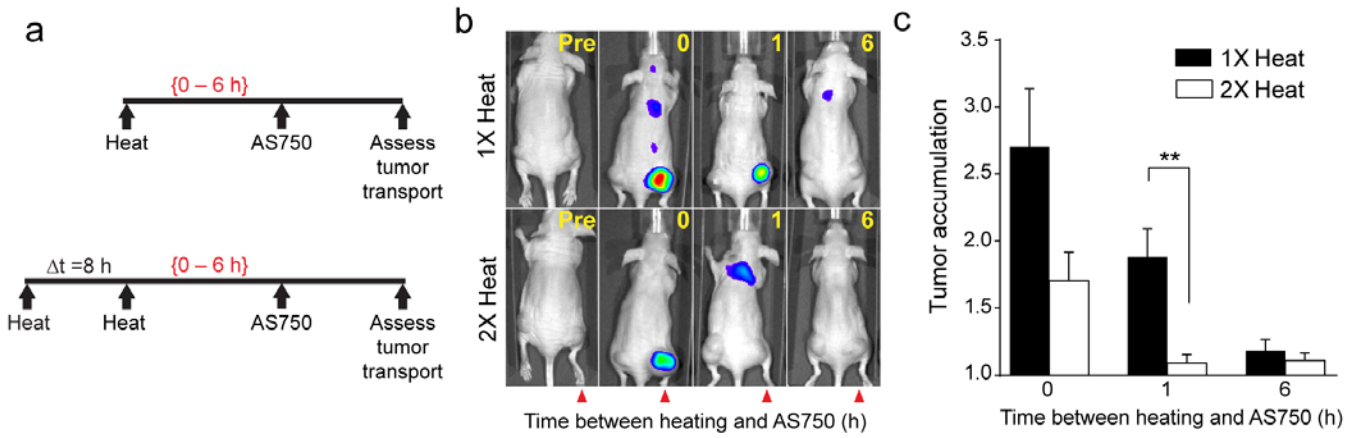

Supplementary Figure 2. Diminished window of tumor transport after re-exposure to PEG-NR heating. (a) Experimental time course includes an initial exposure to PEG-NR heating (heat), an interval delta T of 8 h, re-exposure to PEG-NR heating (heat, 2X group), and AS750 administration offset from the final heating by 0, 1, or 6 h. Tumor accumulation is quantified via in vivo fluorescence imaging. (b) Representative in vivo fluorescence images demonstrating shortened window of tumor transport after re-exposure to PEG-NR heating. Red arrows indicate heated tumors. (c) Tumor transport (ratio of AS750 in heated versus unheated tumors) for each cohort with the indicated offset in AS750 administration after re-exposure to heating. (n = 8 per group, **P<0.01, unpaired t-test, two-tailed.) Error bars, SE.

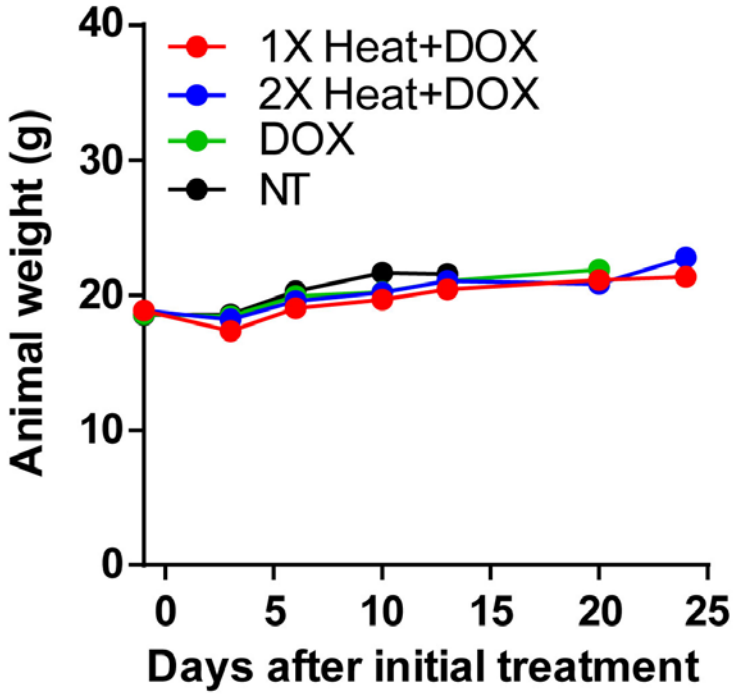

Supplementary Figure 3. Animal weights during PEG-NR and doxorubicin liposome therapeutic trial. Weights remained consistent among treatment groups during the trial period. (n = 8-9 per group) Error bars, SE.

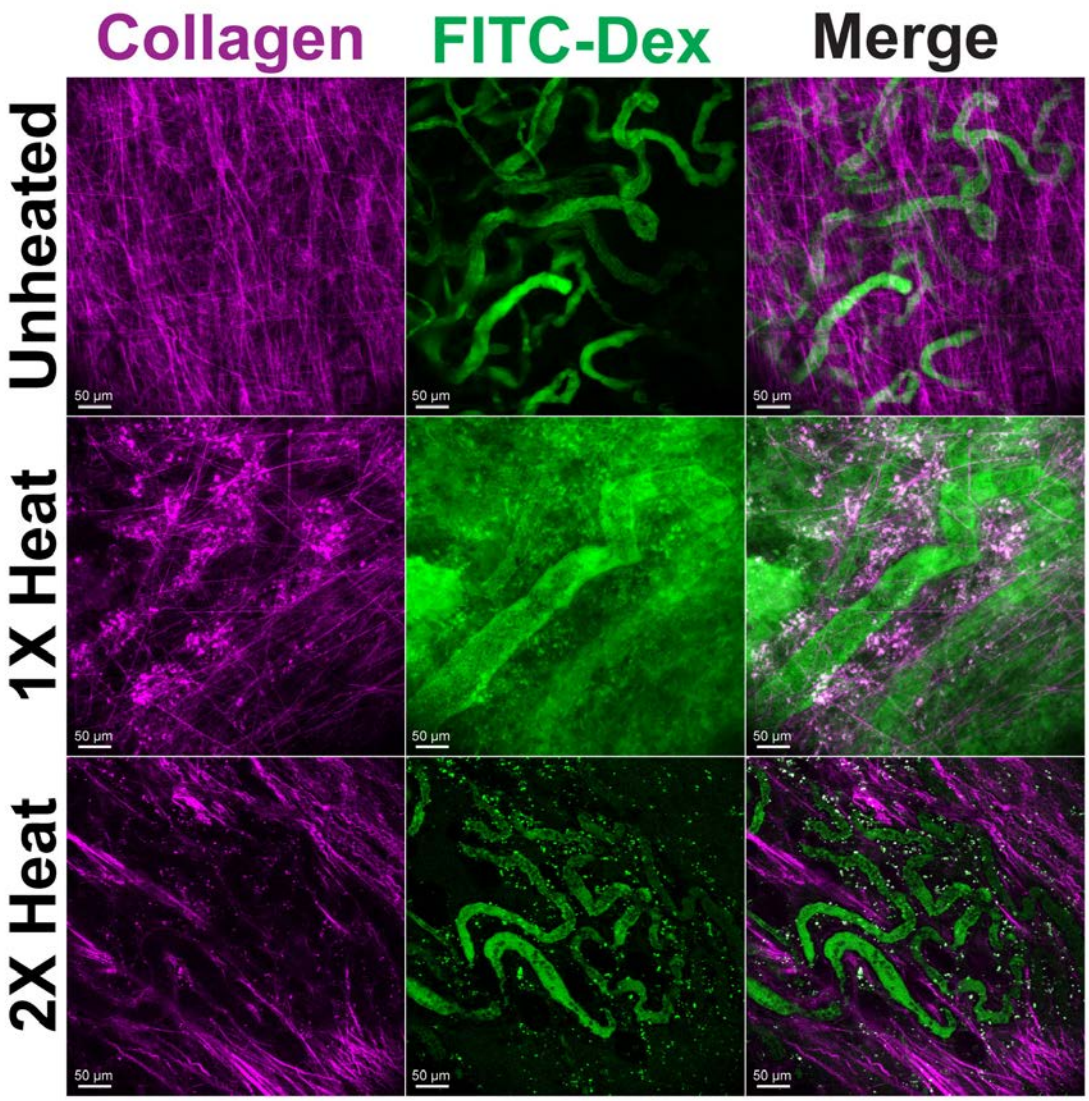

Supplementary Figure 4. Transvascular transport in tumors after single exposure and re-exposure to PEG-NR heating. Unheated and re-exposure (2X heat) tumor vessels display intravascular retention of 70 kDa FITC-Dextran, while a greater degree of extravasation of FITC-Dextran was observed during single exposures (1X heat) to PEG-NR heating. Collagen fibers (magenta) delineate the tumor interstitium and PEG-NRs appear in a punctate perivascular pattern in both channels. (n = 15-31 z-stacks from n = 3-7 animals per treatment group) Scale bar: 50 µm

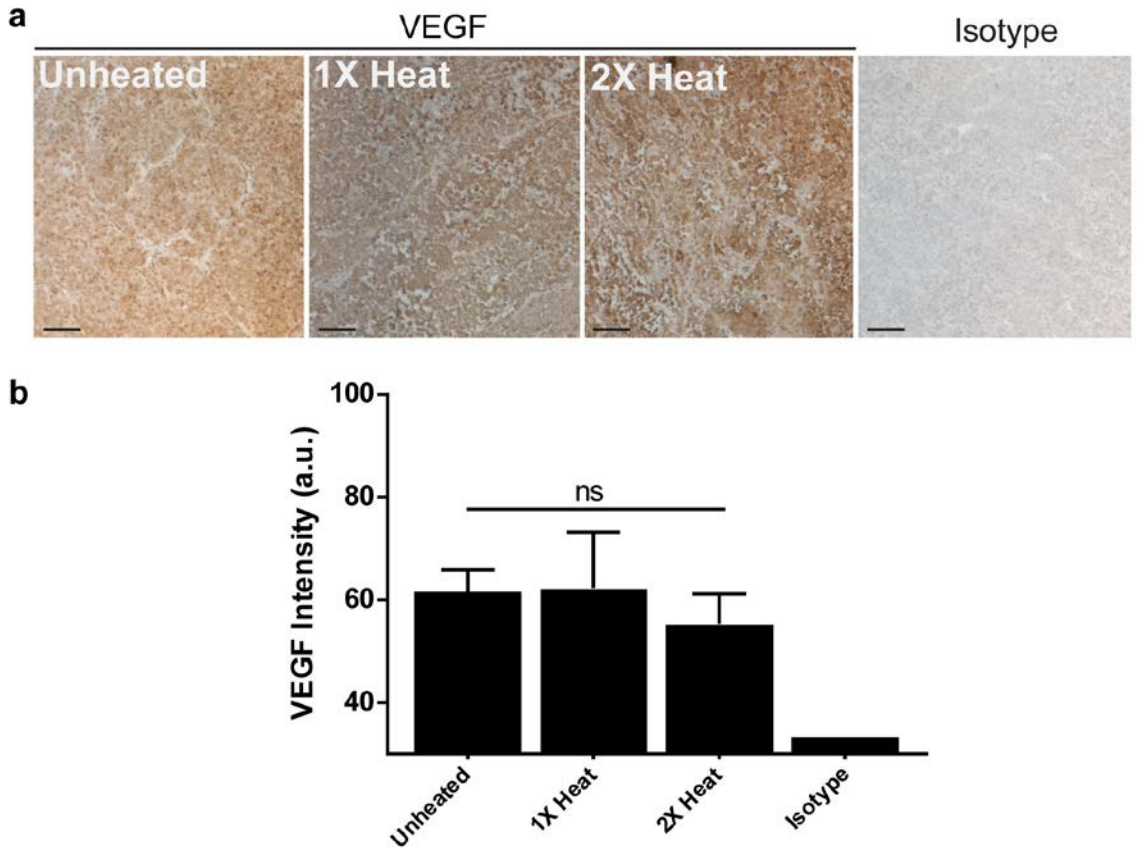

Supplementary Figure 5. Vascular endothelial growth factor (VEGF) expression in PEG-NR heated tumors. (a) Representative images illustrating VEGF expression in tumors either unheated or receiving a single exposure or re-exposure to PEG-NR heating. (b) Mean immunohistochemical staining intensity of large scan images of the tumor cross-sectional area. No significant differences were observed in VEGF intensity between the unheated, single, and repeat PEG-NR heated groups. (n = 4-6 tumors per group) Error bars, SE. Scale bar: 100 µm

a

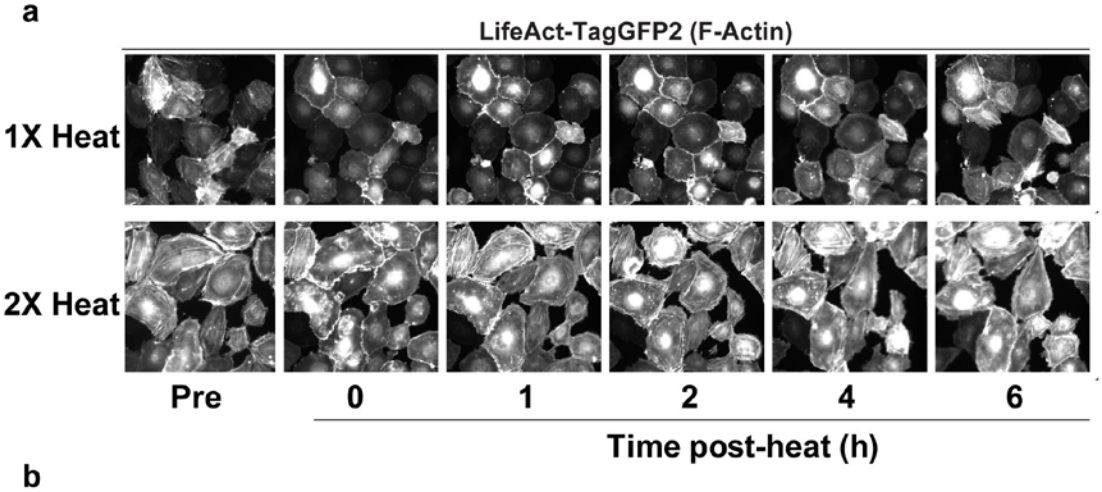

b

Condition	Time Post heat (h)	Fields Examined	Total Cells	Filament-Positive Cells (Mean ± SD)	Total Cells (Mean ± SD)	% Filament-Positive (Mean ± SD)
1X	Pre	6	1072	111.83 ± 15.61	178.67 ± 21.65	62.92 ± 8.14
	0	6	1107	7.83 ± 6.18	184.50 ± 22.47	4.08 ± 3.12
	1	6	1213	6.00 ± 4.20	202.17 ± 10.93	2.97 ± 2.13
	2	6	1172	13.83 ± 8.06	195.33 ± 15.49	7.15 ± 4.45
	4	6	1123	42.67 ± 20.18	187.17 ± 13.32	22.95 ± 11.09
	6	6	1154	57.17 ± 40.18	192.33 ± 17.43	30.39 ± 21.81
2X	Pre	8	1117	101.25 ± 21.40	139.63 ± 13.21	72.62 ± 13.92
	0	8	1161	24.25 ± 8.48	145.13 ± 16.31	16.95 ± 6.22
	1	8	1150	90.88 ± 14.02	143.75 ± 13.71	63.61 ± 10.65
	2	8	1127	106.13 ± 10.86	140.88 ± 15.67	75.87 ± 9.08
	4	8	1099	99.75 ± 16.13	137.38 ± 12.66	72.38 ± 8.27
	6	8	1088	87.00 ± 12.46	136.00 ± 14.79	64.29 ± 9.22

Supplementary Figure 6. Endothelial cell F-Actin dynamics during heat exposure and recovery. (a) Representative images of endothelial F-actin filaments prior to heat exposure and 0 – 6 hours following heating for the single exposure (1X) and re-exposure (2X) groups. Loss of filament structure after heat exposure was observed in both single heat exposure and re-exposure groups, with more efficient recovery of filament structure in the re-exposure group. The same fields were imaged at each time point to enable measurements of actin dynamics in the same cells over time. (b) Quantification of endothelial cells and F-actin structure. A total of 13,583 individual cell measurements were scored for this analysis.

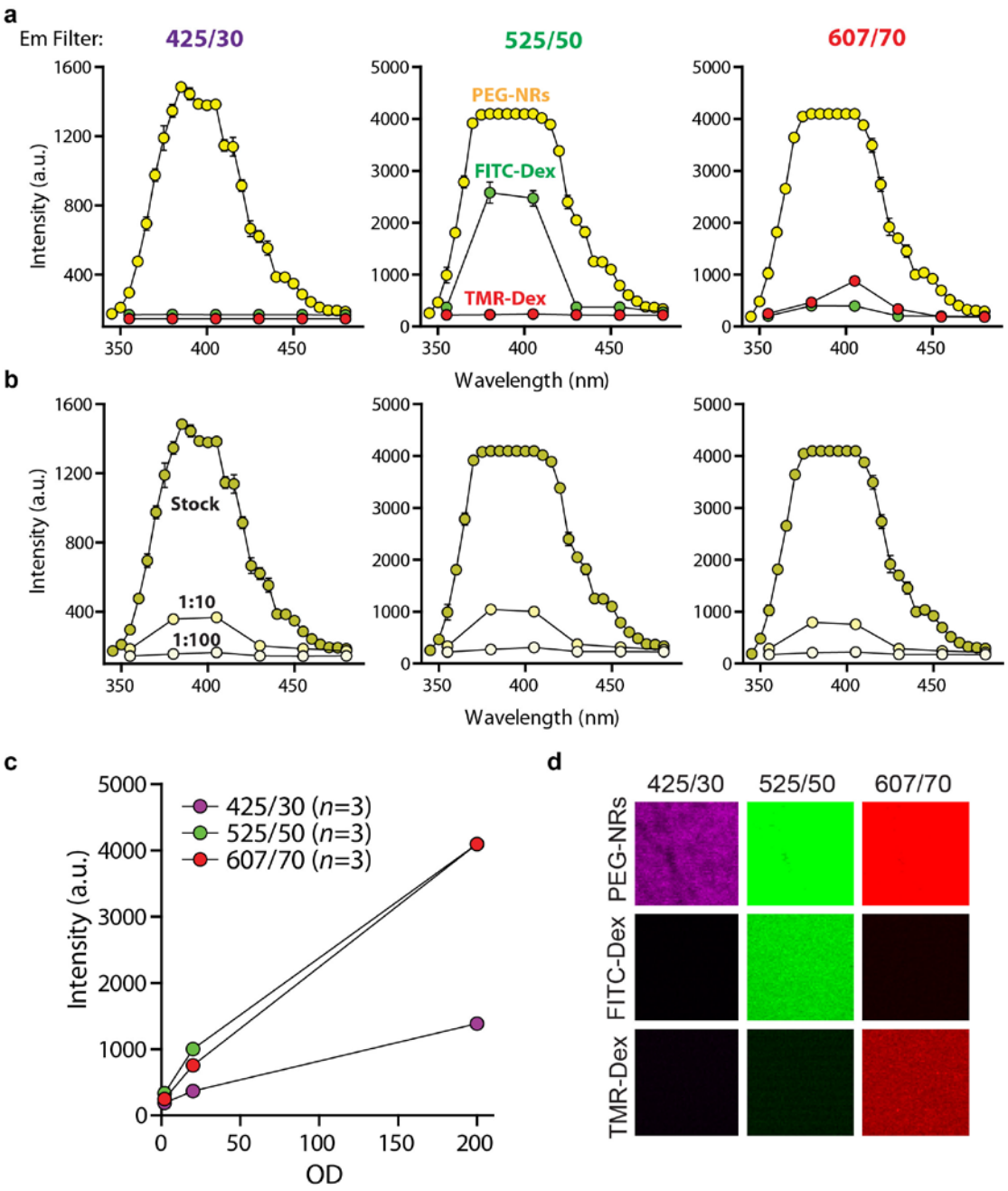

Supplementary Figure 7. Visualizing PEG-NRs in the tumor microenvironment using multiphoton microscopy. (**a**) Fluorescence/luminescence intensities of PEG-NRs (yellow), FITC-Dextran (green), and TMR-Dextran (red) with three separate emission filter channels (425/30, 525/50, and 607/70 nm). An intense signal with a peak at ~400nm was observed for PEG-NRs in all three channels. FITC-Dextran was detected with the 525/50 filter and TMR-Dextran with the 607/70 only. (**b**) Dose-dependent luminescence of PEG-NRs in each channel using 1:10 and 1:100 dilutions from stock PEG-NR concentration (OD: 200). (**c**) Plot of peak intensity versus PEG-NR optical density with each emission filter. (**d**) Images of PEG-NRs, FITC-Dextran, and TMR-Dextran acquired by multiphoton microscopy.

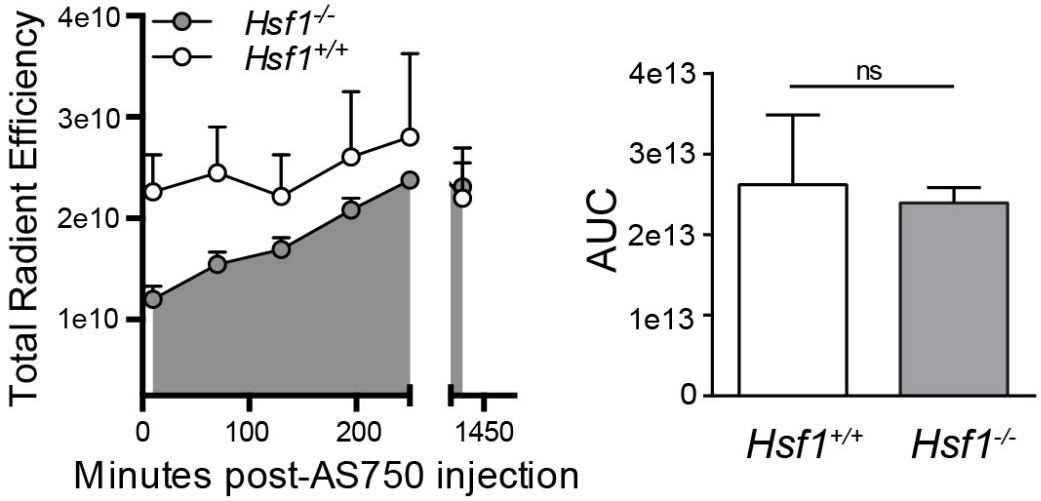

Supplementary Figure 8. Cargo accumulation in tumors with Hsf1+/+ and Hsf1-/- vasculature after single exposure to PEG-NR heating. Kinetics (a) and overall levels (b) of accumulation of AS750 up to 24 hours observed for both groups. Error bars, SE. (n = 3 per group)

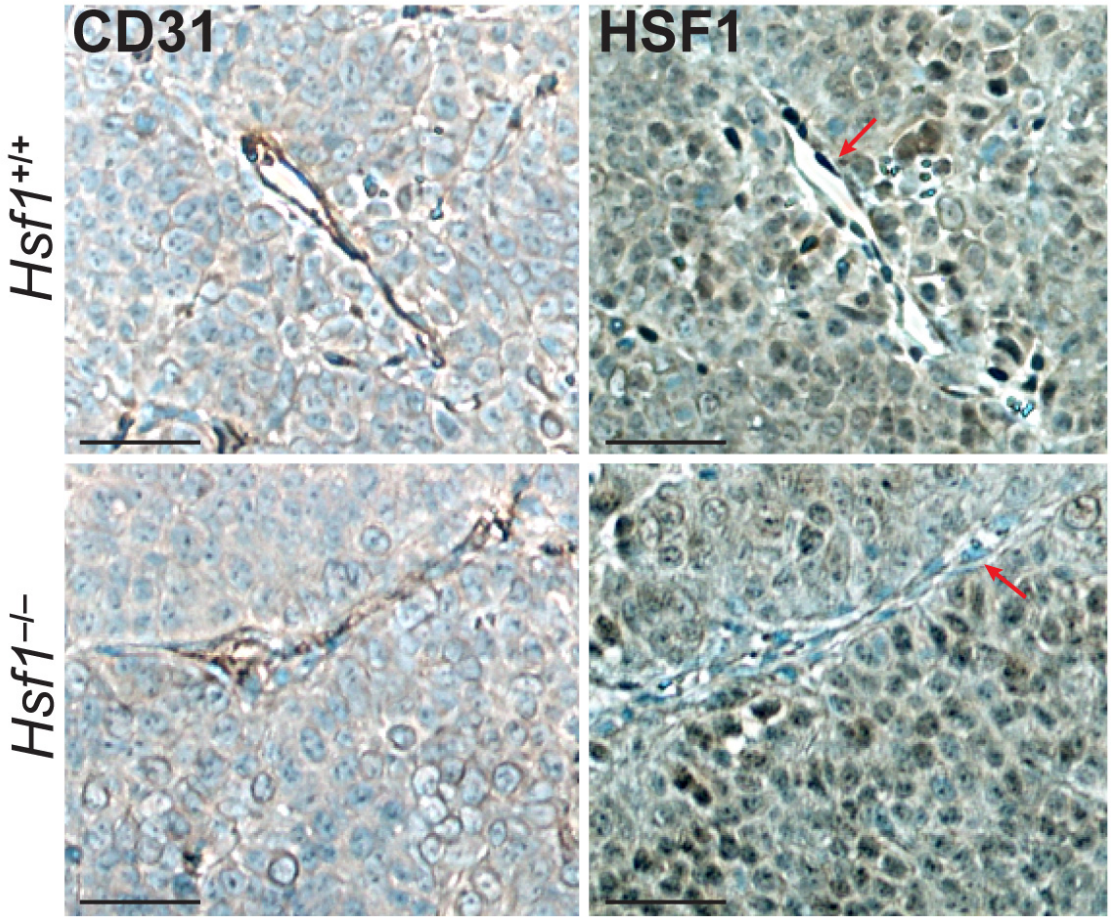

Supplementary Figure 9. HSF1 expression in tumor-associated vasculature following PEG-NR heating. Immunohistochemical staining of serial tissue sections for PECAM-1 (CD31) to label endothelial vessels and HSF1, counterstained with H&E. CD31-positive endothelium in *Hsf1*+/+ models displays a strong nuclear HSF1 staining pattern (red arrow), consistent with HSF1 activation and translocation to the nucleus with PEG-NR heating. CD31-positive endothelium in *Hsf1*-/- models displayed no observable HSF1 staining pattern (red arrow). In both models, positive HSF1 staining was detected in tumor parenchymal cells. Scale bar: 100 µm

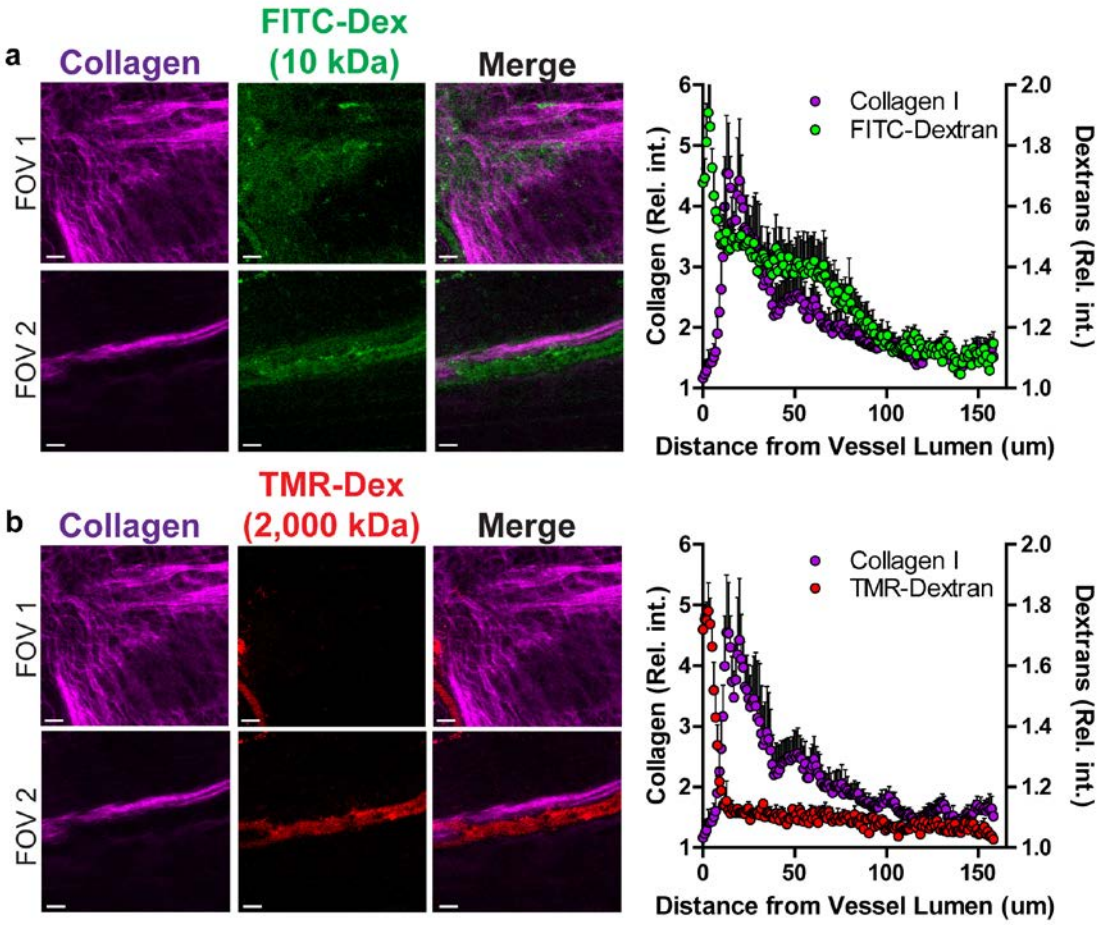

Supplementary Figure 10. Size-dependent macromolecular extravasation from the unheated vasculature. Intravenous co-administration of (a) 10 kDa FITC-Dextran and (b) 2,000 kDa TMR-Dextran revealed greater extravasation of the smaller molecular-weight compound, which appeared to become sequestered in regions with dense collagen fibers as shown by the correspondence in relative intensities on line histograms computed for collagen and FITC-Dextran. Larger molecular weight TMR-Dextran was retained within the vessel lumen in the same field of view, revealing the size-dependence of extravasation in our model. Scale bar: 50 μm